

The Magic in Qudit Shadow Estimation based on the Clifford Group

Chengsi Mao,^{1,2,3} Changhao Yi,^{1,2,3} and Huangjun Zhu^{1,2,3,*}

¹*State Key Laboratory of Surface Physics, Department of Physics,
and Center for Field Theory and Particle Physics, Fudan University, Shanghai 200433, China*

²*Institute for Nanoelectronic Devices and Quantum Computing, Fudan University, Shanghai 200433, China*

³*Shanghai Research Center for Quantum Sciences, Shanghai 201315, China*

(Dated: October 18, 2024)

Shadow estimation is a sample-efficient protocol for learning the properties of a quantum system through randomized measurements, but the current understanding on qudit shadow estimation is quite limited compared with the qubit setting. Here we clarify the sample complexity of qudit shadow estimation based on the Clifford group, where the local dimension d is an odd prime. Notably, we show that the overhead of qudit shadow estimation over the qubit counterpart is only $\mathcal{O}(d)$, which is independent of the qudit number n , although the set of stabilizer states may deviate exponentially from a 3-design with respect to the third moment operator. Furthermore, by adding one layer of magic gates, we propose a simple circuit that can significantly boost the efficiency. Actually, a single magic gate can already eliminate the $\mathcal{O}(d)$ overhead in qudit shadow estimation and bridge the gap from the qubit setting.

I. INTRODUCTION

Learning the properties of an unknown quantum system is of both fundamental and practical importance in quantum science and technology. The classical shadow estimation was proposed as a sample-efficient protocol for fulfilling this task [1–4]. Not demanding a full classical description of the quantum state, this protocol circumvents the ‘curse of dimensionality’ of traditional quantum state tomography [5, 6]. Recently, a number of variants have been proposed to make the protocol more robust and practical on NISQ devices. For example, noise calibration [7, 8] and error-mitigation techniques [9, 10] can make shadow estimation noise-resilient. Alternative schemes based on shallow circuits [11–13], locally scrambled unitary ensembles [14, 15], generalized measurements [16, 17], and hybrid framework [18] are also appealing to practical applications. The efficiency of this approach have been demonstrated in a number of experiments [19–21].

The Clifford group is one of the most important groups in quantum information processing and plays a pivotal role in quantum computation, error correction, and randomized benchmarking [3, 22–24]. In the case of qubits, it is particularly appealing to shadow estimation because it forms a unitary 3-design [25, 26] and is thus maximally efficient in important tasks such as fidelity estimation [1]. Recently, estimation protocols based on the Clifford group or its variants have attracted increasing attention and found extensive applications in various estimation problems [11–13, 27–30].

Nevertheless, physical systems as information carriers are not necessarily binary, but typically exhibit multilevel structures, which can be exploited

as a resource [31, 32]. Moreover, such systems may help reduce circuit complexity [33, 34], enhance efficiency in quantum error correction [35] and magic state distillation [36], and improve noise robustness in Bell and steering tests [37–39] and quantum cryptography [40]. Meanwhile, developments on the experimental control of qudit systems with photonics, solid-state, trapped ion, and superconducting platforms have made universal and programmable qudit-based quantum processors possible [41–44]. Understanding the efficiency of qudit shadow estimation is thus of key theoretical and practical interest. However, unlike the qubit counterpart, the qudit Clifford group is not a unitary 3-design [25, 26, 45], which means it is substantially more difficult to understand its performance in shadow estimation. Actually, little is known about this issue so far despite the intensive efforts of many researchers.

In this work we clarify the sample complexity of qudit shadow estimation based on the Clifford group, where the local dimension d is an odd prime. We show that the overhead of qudit shadow estimation over the qubit counterpart is only $\mathcal{O}(d)$, which is independent of the system size n , although the set of stabilizer states may deviate exponentially from a 3-design with respect to the third moment operator when $d \neq 2 \pmod{3}$. Furthermore, by adding one layer of magic gates, we propose a simple circuit that can significantly boost the efficiency in shadow estimation. Surprisingly, a single magic gate can already eliminate the $\mathcal{O}(d)$ overhead in qudit shadow estimation and bridge the gap between qudit systems and qubit systems. Notably, the sample complexity of fidelity estimation is independent of the local dimension and qudit number. To corroborate these theoretical findings, we develop a complete simulation algorithm on qudit shadow estimation based on the Clifford group supplemented by magic gates. Our work shows that the distinction between the qudit

* zhu Huangjun@fudan.edu.cn

Clifford group and qubit Clifford group is not so serious to quantum information processing. Meanwhile, this work highlights the power of a single magic gate in a practical quantum information task, which has not been fully appreciated before.

Our main results are based on a deep understanding of the third moments of Clifford orbits, including the orbits of stabilizer states and magic states in particular. The main proofs of Theorems 2-4 and relevant technical details are presented in our companion paper [46], which builds on the previous work [47].

II. SHADOW ESTIMATION

Suppose the Hilbert space \mathcal{H} is a tensor power of the form $\mathcal{H} = \mathcal{H}_d^{\otimes n}$, where the local dimension d is a prime, and the total dimension is $D = d^n$. The computational basis of $\mathcal{H}_d^{\otimes n}$ can be labeled by elements in \mathbb{F}_d^n , where \mathbb{F}_d is the finite field composed of d elements. Our main task is to estimate the expectation values of certain linear operators on $\mathcal{H}_d^{\otimes n}$ with respect to an unknown n -qudit quantum state ρ . To this end, we can repeatedly apply a random unitary U sampled from a pre-selected ensemble \mathcal{E} to rotate the state ($\rho \mapsto U\rho U^\dagger$), followed by a computational-basis measurement with outcome $\mathbf{b} \in \mathbb{F}_d^n$. This procedure defines a quantum channel as follows, $\mathcal{M}(\rho) := \mathbb{E}[U^\dagger|\mathbf{b}\rangle\langle\mathbf{b}|U]$, and the inverse \mathcal{M}^{-1} is called the reconstruction map. By virtue of this map we can construct an estimator $\hat{\rho} := \mathcal{M}^{-1}(U^\dagger|\mathbf{b}\rangle\langle\mathbf{b}|U)$, called a (classical) shadow of ρ , in each run [1].

Suppose we want to estimate the expectation value of an operator \mathfrak{D} on $\mathcal{H}_d^{\otimes n}$. If N samples are available, then an unbiased estimator \hat{o} for $o := \text{tr}(\mathfrak{D}\rho)$ can be constructed from the empirical mean,

$$\hat{o} = \frac{1}{N} \sum_{j=1}^N \hat{o}_j = \frac{1}{N} \sum_{j=1}^N \text{tr}(\mathfrak{D}\hat{\rho}_j), \quad (1)$$

where $\hat{\rho}_j$ is the estimator for ρ in the j th run. The MSE (Mean Square Error) of \hat{o} only depends on the traceless part $\mathfrak{D}_0 = \mathfrak{D} - \text{tr}(\mathfrak{D})\mathbb{I}/D$ of \mathfrak{D} [1], where \mathbb{I} is the identity operator on $\mathcal{H}_d^{\otimes n}$. It can be upper bounded as follows (see Appendix A for a proof),

$$\langle \varepsilon^2 \rangle \leq \frac{\|\mathfrak{D}_0\|_{\text{sh}}^2}{N}, \quad (2)$$

where the (squared) shadow norm $\|\mathfrak{D}\|_{\text{sh}}^2$ reads [1]

$$\max_{\sigma} \mathbb{E}_{U \sim \mathcal{E}} \sum_{\mathbf{b} \in \mathbb{F}_d^n} \langle \mathbf{b}|U\sigma U^\dagger|\mathbf{b}\rangle \cdot \left| \langle \mathbf{b}|U\mathcal{M}^{-1}(\mathfrak{D})U^\dagger|\mathbf{b}\rangle \right|^2. \quad (3)$$

The maximization is over all quantum states on $\mathcal{H}_d^{\otimes n}$. Alternatively, we can use the median of means estimation to decrease the probability of large deviation

from the true value. Generalization to two or more observables is also straightforward. In any case, the shadow norm plays a central role in the analysis of the sample complexity and is widely used as the key figure of merit for evaluating the performance of a shadow estimation protocol.

When the ensemble \mathcal{E} of unitaries is a 2-design, the associated reconstruction map takes on a simple form, $\mathcal{M}^{-1}(\mathfrak{D}) = (D+1)\mathfrak{D} - \text{tr}(\mathfrak{D})\mathbb{I}$ for any linear operator \mathfrak{D} acting on $\mathcal{H}_d^{\otimes n}$. If in addition \mathcal{E} is a 3-design, then $\|\mathfrak{D}_0\|_{\text{sh}}^2 \leq 3\|\mathfrak{D}_0\|_2^2 [1]$.

III. HEISENBERG-WEYL GROUP AND CLIFFORD GROUP

The phase operator Z and cyclic-shift operator X for a single qudit are defined as follows,

$$Z|j\rangle = \omega_d^j|j\rangle, \quad X|j\rangle = |j+1\rangle, \quad (4)$$

where $\omega_d := e^{\frac{2\pi i}{d}}$, and the addition $j+1$ is modulo d . When d is an odd prime, the qudit Heisenberg-Weyl (HW) group $\mathcal{W}(d)$ is generated by Z and X ; when $d=2$, the HW group $\mathcal{W}(d)$ reduces to the Pauli group and is generated by Z , X , and iI , where I is the identity operator on \mathcal{H}_d . The n -qudit HW group $\mathcal{W}(n, d)$ is the tensor product of n copies of $\mathcal{W}(d)$, and its elements are called Weyl operators. A Weyl operator is trivial if it is proportional to the identity and nontrivial otherwise. It is m -local if it is a tensor product of m nontrivial single-qudit Weyl operators and $(n-m)$ identity operators on \mathcal{H}_d .

The single-qudit Clifford group $\text{Cl}(d)$ is the normalizer of the HW group $\mathcal{W}(d)$. The local Clifford group $\text{Cl}(d)^{\otimes n}$ is the tensor product of n copies of $\text{Cl}(d)$. By contrast, the (global) Clifford group $\text{Cl}(n, d)$ is the normalizer of $\mathcal{W}(n, d)$. When $d=2$, the Clifford group $\text{Cl}(n, d)$ is a 3-design [25, 26], and this is the only known infinite family of 3-designs based on discrete groups. Indeed, the performance guarantee of qubit shadow estimation is rooted in the 3-design property of $\text{Cl}(n, 2)$. When d is an odd prime, the Clifford group $\text{Cl}(n, d)$ is only a 2-design [25, 26], and little is known about the efficiency of qudit shadow estimation based on the Clifford group, which motivates the current study.

IV. SHADOW ESTIMATION BASED ON LOCAL CLIFFORD MEASUREMENTS

First, we choose the local Clifford group for shadow estimation, i.e., $\mathcal{E} = \text{Cl}(d)^{\otimes n}$. This is the qudit generalization of the scheme based on ‘random Pauli measurements’ in qubit shadow estimation [1]. The

associated reconstruction map reads

$$\mathcal{M}^{-1}(U^\dagger|\mathbf{b}\rangle\langle\mathbf{b}|U) = \bigotimes_{j=1}^n [(d+1)U_j^\dagger|b_j\rangle\langle b_j|U_j - I]. \quad (5)$$

On this basis we can determine the basic properties of the shadow norm as summarized in Proposition 1 and Theorem 1 below; see Appendix C for proofs. Proposition 1 also follows from Theorem 4 in the companion paper [46]. As in the qubit case, this strategy is efficient if \mathfrak{D} only acts on a few qudits.

Proposition 1. *Suppose \mathfrak{D} is an m -local Weyl operator with $m \geq 1$. Then its shadow norm associated with local Clifford measurements reads*

$$\|\mathfrak{D}\|_{\text{sh}}^2 = (d+1)^m. \quad (6)$$

Theorem 1. *Suppose \mathfrak{D} is an m -local linear operator on $\mathcal{H}_d^{\otimes n}$, that is, $\mathfrak{D} = \tilde{\mathfrak{D}} \otimes I^{\otimes(n-m)}$ with $\tilde{\mathfrak{D}}$ acting on $\mathcal{H}_d^{\otimes m}$. Then its shadow norm associated with local Clifford measurements satisfies*

$$\|\mathfrak{D}\|_{\text{sh}}^2 \leq d^m \|\tilde{\mathfrak{D}}\|_2^2. \quad (7)$$

V. SHADOW ESTIMATION BASED ON GLOBAL CLIFFORD MEASUREMENTS

Next, we turn to shadow estimation based on the global Clifford group, i.e., $\mathcal{E} = \text{Cl}(n, d)$. Equivalently, the associated measurement primitive is the orbit $\text{Stab}(n, d)$ of all n -qudit stabilizer states. Since the Clifford group $\text{Cl}(n, d)$ forms a unitary 2-design, any Clifford orbit forms a 2-design, and the corresponding reconstruction map is particularly simple,

$$\mathcal{M}^{-1}(U^\dagger|\mathbf{b}\rangle\langle\mathbf{b}|U) = (D+1)U^\dagger|\mathbf{b}\rangle\langle\mathbf{b}|U - \mathbb{I}. \quad (8)$$

However, $\text{Stab}(n, d)$ does not form a 3-design when d is an odd prime [45], and it is substantially more difficult to determine the shadow norm of a generic observable. Indeed, a deep understanding of the third moment of stabilizer states is indispensable to resolve this problem. In the companion paper [46] we have clarified the properties of the third moment, which enables us to derive universal upper bounds for the shadow norm as shown in the following theorem. A sketch of the proof is presented in Appendix E.

Theorem 2. *Suppose $\mathcal{E} = \text{Cl}(n, d)$ and \mathfrak{D} is a traceless linear operator on $\mathcal{H}_d^{\otimes n}$. Then*

$$\|\mathfrak{D}\|_2^2 \leq \|\mathfrak{D}\|_{\text{sh}}^2 \leq (2d-3)\|\mathfrak{D}\|_2^2 + 2\|\mathfrak{D}\|^2. \quad (9)$$

If \mathfrak{D} is diagonal in a stabilizer basis, then

$$\|\mathfrak{D}\|_{\text{sh}}^2 \leq (d-1)\|\mathfrak{D}\|_2^2 + d\|\mathfrak{D}\|^2. \quad (10)$$

If $n = 1$ and \mathfrak{D} is diagonal in a stabilizer basis, then

$$\|\mathfrak{D}\|_{\text{sh}}^2 = (d+1)\|\mathfrak{D}\|^2. \quad (11)$$

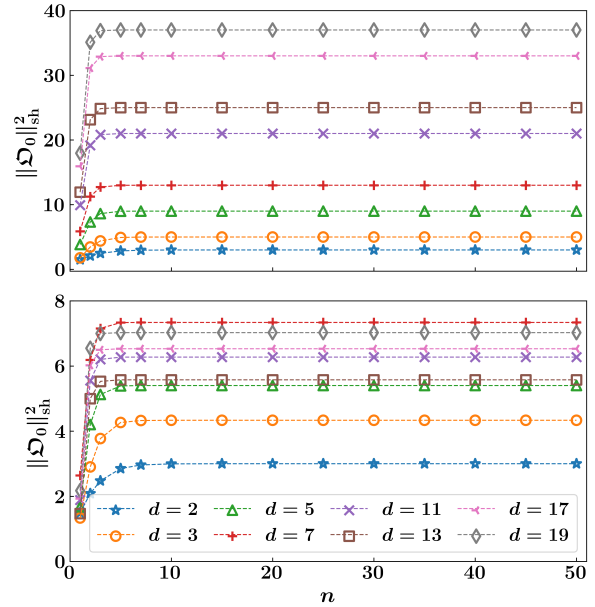


FIG. 1. Shadow norm associated with the projector \mathfrak{D} onto a stabilizer state with respect to the Clifford circuit (upper plot) and Clifford circuit supplemented by one canonical T gate (lower plot). Here \mathfrak{D}_0 denotes the traceless part of \mathfrak{D} .

Incidentally, Eq. (11) implies Proposition 1. Thanks to Theorem 2, the ratio $\|\mathfrak{D}\|_{\text{sh}}^2/\|\mathfrak{D}\|_2^2$ is upper bounded by $2d-1$, which is independent of the qudit number n , so the overhead of shadow estimation for a qudit system over a qubit system does not grow with n . This result may have profound implications for quantum information processing based on qudits, and is quite unexpected given that $\text{Stab}(n, d)$ is not a 3-design. In fact, the operator norm of the third normalized moment operator of $\text{Stab}(n, d)$ increases exponentially with n when $d \not\equiv 2 \pmod{3}$ [46]. Surprisingly, measurement ensembles far from 3-designs (with respect to one of the most popular figures of merit) can achieve similar performances as 3-designs in shadow estimation. When $n = 1$, $\text{Stab}(n, d)$ forms a complete set of mutually unbiased bases, so Eq. (11) is also instructive to understanding shadow estimation based on mutually unbiased bases.

When \mathfrak{D} is a stabilizer projector, we can even derive an analytic formula for $\|\mathfrak{D}_0\|_{\text{sh}}^2$.

Theorem 3. *Suppose $\mathcal{E} = \text{Cl}(n, d)$ and \mathfrak{D} is a rank- K stabilizer projector on $\mathcal{H}_d^{\otimes n}$ with $1 \leq K \leq d^{n-1}$. Then*

$$\frac{\|\mathfrak{D}_0\|_{\text{sh}}^2}{\|\mathfrak{D}_0\|_2^2} = \frac{D+1}{D+d} \left(d-1 - \frac{d}{D} + \frac{d}{K} \right). \quad (12)$$

The shadow norm $\|\mathfrak{D}_0\|_{\text{sh}}^2$ increases linearly with the local dimension d , but is almost independent of n when $n \geq 5$, as illustrated in Fig. 1 for the

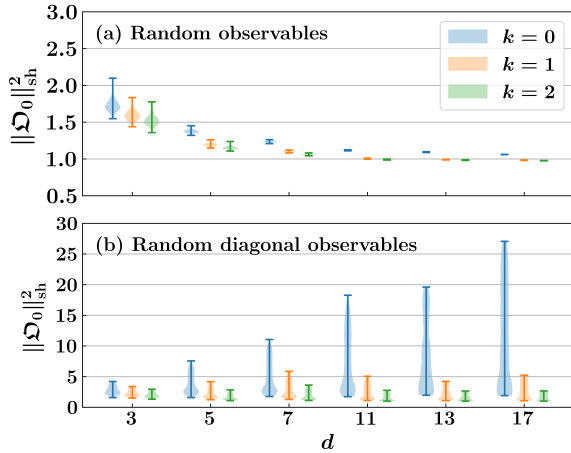


FIG. 2. Distributions of the shadow norms of random two-qudit traceless observables (a) and random two-qudit traceless diagonal observables (b) that are normalized with respect to the Hilbert-Schmidt norm. The unitary ensemble \mathcal{E} is based on the Clifford circuit supplemented by k canonical T gates.

case $K = 1$, so that \mathcal{D} is the projector onto a stabilizer state. In addition, $\|\mathcal{D}_0\|_{\text{sh}}^2$ can saturate the upper bounds in Eqs. (9) and (10) asymptotically as $n \rightarrow \infty$. Interestingly, stabilizer states are the most difficult to estimate by stabilizer measurements. For comparison, Fig. 2 shows the distributions of shadow norms of random observables and random diagonal observables of two qudits that are normalized with respect to the Hilbert-Schmidt norm (here all observables are Hermitian and traceless). In the former case, the shadow norms are usually much smaller than the upper bound in Eq. (9) and do not increase with the local dimension; in the later case, by contrast, the upper bound in Eq. (10) is nearly tight.

VI. THE POWER OF MAGIC GATES IN SHADOW ESTIMATION

Clifford circuits supplemented by sufficiently many magic gates can realize universal quantum computation, but little is known about the power of limited magic gates in quantum information processing. Here we propose a simple recipe for boosting the efficiency of qudit shadow estimation by virtue of a few magic gates and show that a single magic gate can already bridge the gap between a qudit system and a qubit system.

We are mainly interested in qudit magic gates that are diagonal in the computational basis and belong to the third Clifford hierarchy [48], which are referred to as T gates henceforth. Up to an irrelevant global

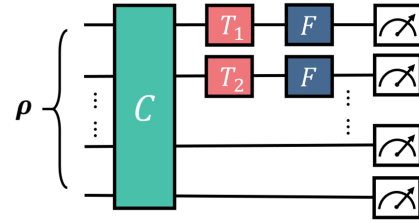


FIG. 3. A Clifford circuit supplemented by one layer of T gates, which is useful for shadow estimation.

phase factor, a qudit T gate takes on the form [46, 49]

$$T := \sum_{b \in \mathbb{F}_d} \tilde{\omega}^{f(b)} |b\rangle\langle b|, \quad \tilde{\omega} := \begin{cases} \omega_d & d \geq 5, \\ \omega_9 & d = 3. \end{cases} \quad (13)$$

When $d \geq 5$, f is a cubic polynomial on \mathbb{F}_d ; when $d = 3$, $f(b) = c_3 b^3 + 3c_2 b^2$ (with $c_2 \in \mathbb{F}_3$, $c_3 \in \mathbb{Z}_9$ and $c_3 \neq 0 \pmod{3}$) is a function from \mathbb{F}_3 to \mathbb{Z}_9 . The T gate associated with the function $f(b) = b^3$ is referred to as the canonical T gate henceforth.

Using T gates we can construct an alternative unitary ensemble for shadow estimation as illustrated in Fig. 3: First apply a random Clifford unitary C in $\text{Cl}(n, d)$, then apply T gates on k different qudits (the first k qudits for simplicity), each followed by a Fourier gate F , where

$$F := \frac{1}{\sqrt{d}} \sum_{a, b \in \mathbb{F}_d} \omega_d^{ab} |a\rangle\langle b|. \quad (14)$$

Denote by T_j the T gate applied to the j th qudit and by $\mathcal{E}(\{T_j\}_{j=1}^k)$ the resulting unitary ensemble. The effective measurement ensemble corresponds to the Clifford orbit generated from a magic state. The circuit we employ is substantially simpler than the popular interleaved Clifford circuits: in each run we need to sample a random Clifford unitary only once, which is as economic as possible and is particularly appealing in the NISQ era [50]. Nevertheless, such simple circuits are surprisingly powerful in shadow estimation as shown in the following theorem; see Appendix E for a proof sketch.

Theorem 4. *Suppose $\mathcal{E} = \mathcal{E}(\{T_j\}_{j=1}^k)$ with $1 \leq k \leq n$, where T_1, T_2, \dots, T_k are T gates, and \mathcal{D} is a traceless linear operator on $\mathcal{H}_d^{\otimes n}$. Then*

$$\|\mathcal{D}_0\|_{\text{sh}}^2 \leq \gamma_{d,k} \|\mathcal{D}_0\|_{\text{sh}}^2, \quad (15)$$

where

$$\gamma_{d,k} := \begin{cases} 3 + \frac{2^{k+1}(d-2)}{d^k} & d \not\equiv 1 \pmod{3}, \\ 3 + \frac{9}{8} \cdot \frac{4^k}{d^{k-1}} & d \equiv 1 \pmod{3}. \end{cases} \quad (16)$$

As the number k of T gates increases, the shadow norm associated with the ensemble $\mathcal{E}(\{T_j\}_{j=1}^k)$ converges exponentially to the counterpart of a unitary

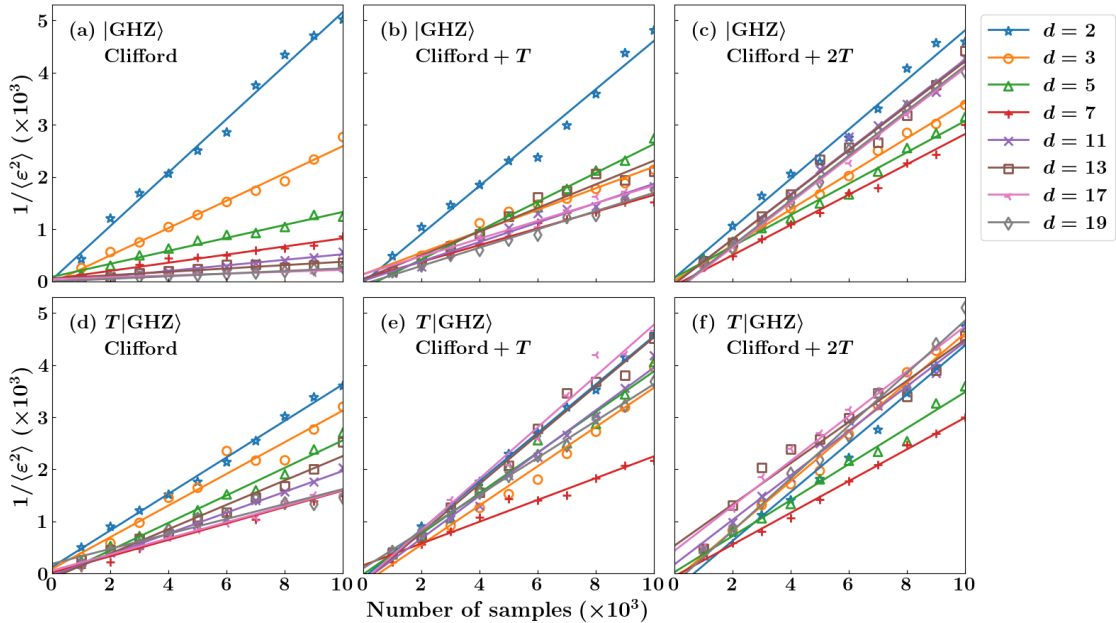


FIG. 4. Simulation results on the inverse MSE in fidelity estimation in which the input state and target state are identical n -qudit GHZ state $|\text{GHZ}\rangle = |\text{GHZ}(n, d)\rangle$ with $n = 100$. The estimation protocols are based on the Clifford circuit supplemented by up to two canonical T gates. The MSE $\langle \varepsilon^2 \rangle$ for each data point is the average over 100 runs. The solid lines are determined by interpolation. Results on the state $T|\text{GHZ}\rangle$ are also shown for comparison.

3-design. Moreover, a single T gate can already bridge the gap between a qudit system and a qubit system. Notably, if the observable \mathfrak{D} has a bounded Hilbert–Schmidt norm, which is the case for many tasks, such as fidelity estimation, then the sample complexity is independent of the local dimension d and qudit number n .

When \mathfrak{D} is a stabilizer projector, we can even derive an analytical formula for $\|\mathfrak{D}_0\|_{\text{sh}}^2$; see our companion paper [46] for details. The results on projectors onto stabilizer states are shown in Fig. 1 (see also Figs. 6 and 7 in Appendix F). In addition, T gates can significantly reduce the shadow norms of random diagonal observables, as illustrated in Fig. 2, although their utility for general random observables seems limited because Clifford circuits are already good enough. Theorem 4 is applicable irrespective of the specific choices of T gates. If we can make educated choices, then the shadow norm $\|\mathfrak{D}_0\|_{\text{sh}}$ can be reduced further as shown in Appendix F.

VII. NUMERICAL SIMULATION

To corroborate our theoretical findings, we performed extensive numerical simulation on qudit shadow estimation based on the Clifford circuit supplemented by a layer of T gates. To this end, we generalize the tableau representation of stabilizer states [51] and gadgetization method for insertion of magic gates in the Clifford circuit [52, 53]

to the qudit setting (see Appendix G for more details). Together with the sampling algorithm of Clifford unitaries [54, 55], we are able to simulate a single shot in shadow estimation on a classical computer with an approximate computational cost of $\mathcal{O}((n+t)^3 + td^{t+1})$, where t is the number of magic gates in the gadgetized circuit.

As a showcase, we consider the task of fidelity estimation in which the input state ρ is identical to a pure target state $|\Psi\rangle\langle\Psi|$. In this case, the observable of interest is $\mathfrak{D} = |\Psi\rangle\langle\Psi|$ and the true fidelity is $\text{tr}(\rho\mathfrak{D}) = 1$. Estimators for the fidelity can be constructed from empirical means as in Eq. (1). First, we test our protocols on the n -qudit GHZ state, that is, $|\Psi\rangle = |\text{GHZ}(n, d)\rangle$ with

$$|\text{GHZ}(n, d)\rangle := \frac{1}{\sqrt{d}} \sum_{b=0}^{d-1} |b\rangle^{\otimes n}. \quad (17)$$

In numerical simulation we set $n = 100$, but the number of qudits has little influence on the sample complexity. Figure 4 shows the simulation results on the inverse MSE $1/\langle \varepsilon^2 \rangle$, which increases linearly with the number of samples as expected from Eq. (2). The smaller the shadow norm, the larger the slope of the interpolation line. If we choose the Clifford circuit without T gates for shadow estimation, then the slope is approximately inversely proportional to the local dimension d . If we add one T gate, then the ratio of the maximum slope over the minimum slope is upper bounded by 3, so the dependence on

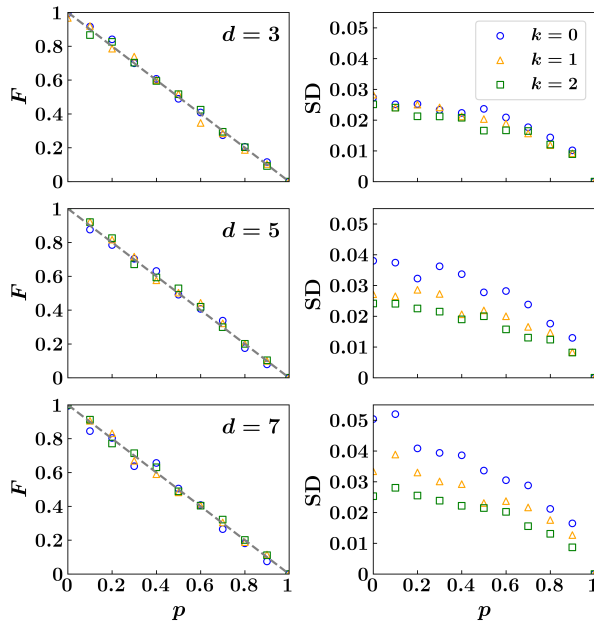


FIG. 5. Fidelity estimated using shadow estimation and the corresponding standard deviation. The target state is the GHZ state in Eq. (17) with $n = 100$, and the input state is the depolarized GHZ state in Eq. (18). The unitary ensemble is based on the Clifford circuit supplemented by k canonical T gates, and the number N of samples is 5000. Each data point for the fidelity is the average over 100 runs, which also determine the standard deviation (SD). The grey lines in the left column show the true fidelity $F = 1 - p + p/D$.

the local dimension is insignificant. If more T gates are applied, then the ratio is even smaller. All these results are consistent with theoretical predictions.

For comparison, we also test our protocols on the state $T|\text{GHZ}(n, d)\rangle$, where T is the canonical T gate acting on the first qudit, and the results are also shown in Fig. 4. Now the MSE gets smaller and we see a ‘duality’ between magic gates in state preparation and in measurements: the MSE is mainly determined by the total number of T gates. Additional simulation results on cluster states and on the median of means estimation can be found in Appendix F; the general conclusions are similar.

Next, we consider a more realistic case in which

the input state is a depolarized GHZ state, that is,

$$\rho = p\mathbb{I}/D + (1 - p)|\text{GHZ}(n, d)\rangle\langle\text{GHZ}(n, d)|, \quad (18)$$

where $0 \leq p \leq 1$, and we want to estimate its fidelity with $|\text{GHZ}(n, d)\rangle$ using shadow estimation. Figure 5 shows that our protocols give quite good estimators for the fidelity using only 5000 samples. Moreover, the fluctuation (standard deviation) gets smaller and smaller as more T gates are added to the Clifford circuit, which agrees with our theoretical prediction.

VIII. SUMMARY

We showed that qudit shadow estimation based on the Clifford group can achieve the same precision as in the qubit setting with only $\mathcal{O}(d)$ overhead in the sample complexity, irrespective of the qudit number. Furthermore, we proposed a simple recipe to boost the efficiency, which requires only one layer of magic gates in addition to the Clifford circuit and is particularly appealing to the NISQ era. Actually, by adding a single magic gate, we can eliminate the $\mathcal{O}(d)$ overhead in qudit shadow estimation and achieve the same sample complexity as in the qubit setting. In this way, we can achieve a constant sample complexity (independent of d and n) in important tasks, such as fidelity estimation. These results means characterization and verification of qudit systems are easier than expected, which may have profound implications for quantum information processing based on qudits. Meanwhile, our work highlights the power of a single magic gate in a practical quantum information task, which is of independent interest and deserves further exploration.

ACKNOWLEDGEMENTS

This work is supported by the National Natural Science Foundation of China (Grant No. 92165109), National Key Research and Development Program of China (Grant No. 2022YFA1404204), and Shanghai Municipal Science and Technology Major Project (Grant No. 2019SHZDZX01).

[1] H.-Y. Huang, R. Kueng, and J. Preskill, Predicting many properties of a quantum system from very few measurements, *Nat. Phys.* **16**, 1050 (2020).
 [2] H.-Y. Huang, Learning quantum states from their classical shadows, *Nat. Rev. Phys.* **4**, 81 (2022).
 [3] M. Kliesch and I. Roth, Theory of quantum system certification, *PRX Quantum* **2**, 010201 (2021).

[4] A. Elben, S. T. Flammia, H.-Y. Huang, R. Kueng, J. Preskill, B. Vermersch, and P. Zoller, The randomized measurement toolbox, *Nat. Rev. Phys.* **5**, 9 (2023).
 [5] J. Haah, A. W. Harrow, Z. Ji, X. Wu, and N. Yu, Sample-optimal tomography of quantum states, in *Proc. Annu. ACM Symp. Theory Comput.* (2016) pp. 913–925.

- [6] M. Cramer, M. B. Plenio, S. T. Flammia, R. Somma, D. Gross, S. D. Bartlett, O. Landon-Cardinal, D. Poulin, and Y.-K. Liu, Efficient quantum state tomography, *Nat. Commun.* **1**, 149 (2010).
- [7] S. Chen, W. Yu, P. Zeng, and S. T. Flammia, Robust shadow estimation, *PRX Quantum* **2**, 030348 (2021).
- [8] D. E. Koh and S. Grewal, Classical shadows with noise, *Quantum* **6**, 776 (2022).
- [9] A. Seif, Z.-P. Cian, S. Zhou, S. Chen, and L. Jiang, Shadow distillation: Quantum error mitigation with classical shadows for near-term quantum processors, *PRX Quantum* **4**, 010303 (2023).
- [10] H. Jnane, J. Steinberg, Z. Cai, H. C. Nguyen, and B. Koczor, Quantum error mitigated classical shadows, *PRX Quantum* **5**, 010324 (2024).
- [11] C. Bertoni, J. Haferkamp, M. Hinsche, M. Ioannou, J. Eisert, and H. Pashayan, Shallow shadows: Expectation estimation using low-depth random Clifford circuits, *Phys. Rev. Lett.* **133**, 020602 (2024).
- [12] M. Ippoliti, Y. Li, T. Rakovszky, and V. Khemani, Operator relaxation and the optimal depth of classical shadows, *Phys. Rev. Lett.* **130**, 230403 (2023).
- [13] T. Schuster, J. Haferkamp, and H.-Y. Huang, Random unitaries in extremely low depth, *arXiv:2407.07754* (2024).
- [14] H.-Y. Hu, S. Choi, and Y.-Z. You, Classical shadow tomography with locally scrambled quantum dynamics, *Phys. Rev. Res.* **5**, 023027 (2023).
- [15] M. C. Tran, D. K. Mark, W. W. Ho, and S. Choi, Measuring arbitrary physical properties in analog quantum simulation, *Phys. Rev. X* **13**, 011049 (2023).
- [16] H. C. Nguyen, J. L. Bönsel, J. Steinberg, and O. Gühne, Optimizing shadow tomography with generalized measurements, *Phys. Rev. Lett.* **129**, 220502 (2022).
- [17] L. Innocenti, S. Lorenzo, I. Palmisano, F. Albarelli, A. Ferraro, M. Paternostro, and G. M. Palma, Shadow tomography on general measurement frames, *PRX Quantum* **4**, 040328 (2023).
- [18] Y. Zhou and Z. Liu, A hybrid framework for estimating nonlinear functions of quantum states, *Npj Quantum Inf.* **10**, 62 (2024).
- [19] G. Struchalin, Y. A. Zagorovskii, E. Kovlakov, S. Straupe, and S. Kulik, Experimental estimation of quantum state properties from classical shadows, *PRX Quantum* **2**, 010307 (2021).
- [20] T. Zhang, J. Sun, X.-X. Fang, X.-M. Zhang, X. Yuan, and H. Lu, Experimental quantum state measurement with classical shadows, *Phys. Rev. Lett.* **127**, 200501 (2021).
- [21] R. Stricker, M. Meth, L. Postler, C. Edmunds, C. Ferrie, R. Blatt, P. Schindler, T. Monz, R. Kueng, and M. Ringbauer, Experimental single-setting quantum state tomography, *PRX Quantum* **3**, 040310 (2022).
- [22] D. Gottesman, *Stabilizer codes and quantum error correction*, Ph.D. thesis, California Institute of Technology (1997).
- [23] M. A. Nielsen and I. L. Chuang, *Quantum computation and quantum information* (Cambridge university press, 2010).
- [24] J. Eisert, D. Hangleiter, N. Walk, I. Roth, D. Markham, R. Parekh, U. Chabaud, and E. Kashefi, Quantum certification and benchmarking, *Nat. Rev. Phys.* **2**, 382 (2020).
- [25] H. Zhu, Multiqubit Clifford groups are unitary 3-designs, *Phys. Rev. A* **96**, 062336 (2017).
- [26] Z. Webb, The Clifford group forms a unitary 3-design, *Quantum Info. Comput.* **16**, 1379 (2016).
- [27] J. Helsen and M. Walter, Thrifty shadow estimation: Reusing quantum circuits and bounding tails, *Phys. Rev. Lett.* **131**, 240602 (2023).
- [28] H.-Y. Huang, Y. Tong, D. Fang, and Y. Su, Learning many-body Hamiltonians with Heisenberg-limited scaling, *Phys. Rev. Lett.* **130**, 200403 (2023).
- [29] H.-Y. Huang, S. Chen, and J. Preskill, Learning to predict arbitrary quantum processes, *PRX Quantum* **4**, 040337 (2023).
- [30] R. Levy, D. Luo, and B. K. Clark, Classical shadows for quantum process tomography on near-term quantum computers, *Phys. Rev. Res.* **6**, 013029 (2024).
- [31] T.-C. Wei, I. Affleck, and R. Raussendorf, Affleck-Kennedy-Lieb-Tasaki state on a honeycomb lattice is a universal quantum computational resource, *Phys. Rev. Lett.* **106**, 070501 (2011).
- [32] M. Ringbauer, M. Meth, L. Postler, R. Stricker, R. Blatt, P. Schindler, and T. Monz, A universal qudit quantum processor with trapped ions, *Nat. Phys.* **18**, 1053 (2022).
- [33] Y. Wang, Z. Hu, B. C. Sanders, and S. Kais, Qudits and high-dimensional quantum computing, *Front. Phys.* **8**, 589504 (2020).
- [34] J. Chu, X. He, Y. Zhou, J. Yuan, L. Zhang, Q. Guo, Y. Hai, Z. Han, C.-K. Hu, W. Huang, *et al.*, Scalable algorithm simplification using quantum AND logic, *Nat. Phys.* **19**, 126 (2023).
- [35] E. T. Campbell, Enhanced fault-tolerant quantum computing in d -level systems, *Phys. Rev. Lett.* **113**, 230501 (2014).
- [36] E. T. Campbell, H. Anwar, and D. E. Browne, Magic-state distillation in all prime dimensions using quantum Reed-Muller codes, *Phys. Rev. X* **2**, 041021 (2012).
- [37] D. Collins, N. Gisin, N. Linden, S. Massar, and S. Popescu, Bell inequalities for arbitrarily high-dimensional systems, *Phys. Rev. Lett.* **88**, 040404 (2002).
- [38] T. Vértesi, S. Pironio, and N. Brunner, Closing the detection loophole in Bell experiments using qudits, *Phys. Rev. Lett.* **104**, 060401 (2010).
- [39] V. Srivastav, N. H. Valencia, W. McCutcheon, S. Leedumrongwatthanakun, S. Designolle, R. Uola, N. Brunner, and M. Malik, Quick quantum steering: Overcoming loss and noise with qudits, *Phys. Rev. X* **12**, 041023 (2022).
- [40] N. J. Cerf, M. Bourennane, A. Karlsson, and N. Gisin, Security of quantum key distribution using d -level systems, *Phys. Rev. Lett.* **88**, 127902 (2002).
- [41] S. Choi, J. Choi, R. Landig, G. Kucsko, H. Zhou, J. Isoya, F. Jelezko, S. Onoda, H. Sumiya, V. Khemani, *et al.*, Observation of discrete time-crystalline order in a disordered dipolar many-body system, *Nature* **543**, 221 (2017).
- [42] M. Erhard, M. Krenn, and A. Zeilinger, Advances in high-dimensional quantum entanglement, *Nat. Rev. Phys.* **2**, 365 (2020).

- [43] Y. Chi, J. Huang, Z. Zhang, J. Mao, Z. Zhou, X. Chen, C. Zhai, J. Bao, T. Dai, H. Yuan, *et al.*, A programmable qudit-based quantum processor, *Nat. Commun.* **13**, 1166 (2022).
- [44] A. Cervera-Lierta, M. Krenn, A. Aspuru-Guzik, and A. Galdá, Experimental high-dimensional Greenberger-Horne-Zeilinger entanglement with superconducting transmon qutrits, *Phys. Rev. Appl.* **17**, 024062 (2022).
- [45] R. Kueng and D. Gross, Qubit stabilizer states are complex projective 3-designs, arXiv:1510.02767 (2015).
- [46] H. Zhu, C. Mao, and C. Yi, Third moments of qudit Clifford orbits and 3-designs based on magic orbits, to be posted (2024).
- [47] D. Gross, S. Nezami, and M. Walter, Schur-Weyl duality for the Clifford group with applications: Property testing, a robust Hudson theorem, and de Finetti representations, *Commun. Math. Phys.* **385**, 1325 (2021).
- [48] D. Gottesman and I. L. Chuang, Demonstrating the viability of universal quantum computation using teleportation and single-qubit operations, *Nature* **402**, 390 (1999).
- [49] M. Howard and J. Vala, Qudit versions of the qubit $\pi/8$ gate, *Phys. Rev. A* **86**, 022316 (2012).
- [50] J. Preskill, Quantum computing in the NISQ era and beyond, *Quantum* **2**, 79 (2018).
- [51] S. Aaronson and D. Gottesman, Improved simulation of stabilizer circuits, *Phys. Rev. A* **70**, 052328 (2004).
- [52] S. Bravyi and D. Gosset, Improved classical simulation of quantum circuits dominated by Clifford gates, *Phys. Rev. Lett.* **116**, 250501 (2016).
- [53] H. Pashayan, O. Reardon-Smith, K. Korzekwa, and S. D. Bartlett, Fast estimation of outcome probabilities for quantum circuits, *PRX Quantum* **3**, 020361 (2022).
- [54] R. Koenig and J. A. Smolin, How to efficiently select an arbitrary Clifford group element, *J. Math. Phys.* **55**, 122202 (2014).
- [55] M. Heinrich, *On Stabiliser Techniques and Their Application to Simulation and Certification of Quantum Devices*, Ph.D. thesis, University of Cologne (2021).
- [56] D. Gross, Hudson's theorem for finite-dimensional quantum systems, *J. Math. Phys.* **47**, 122107 (2006).
- [57] G. B. Folland, *Harmonic analysis in phase space*, 122 (Princeton university press, 1989).
- [58] A. Weil, Sur certains groupes d'opérateurs unitaires, *Acta Math.* **111**, 143–211 (1964).
- [59] S. Anders and H. J. Briegel, Fast simulation of stabilizer circuits using a graph-state representation, *Phys. Rev. A* **73**, 022334 (2006).
- [60] M. Nest, Classical simulation of quantum computation, the Gottesman-Knill theorem, and slightly beyond, arXiv:0811.0898 (2008).
- [61] E. Van Den Berg, A simple method for sampling random Clifford operators, in *2021 IEEE international conference on quantum computing and engineering (QCE)* (2021) pp. 54–59.
- [62] S. Bravyi and D. Maslov, Hadamard-free circuits expose the structure of the Clifford group, *IEEE Trans. Inform. Theor.* **67**, 4546 (2021).
- [63] S. Bravyi, D. Browne, P. Calpin, E. Campbell, D. Gosset, and M. Howard, Simulation of quantum circuits by low-rank stabilizer decompositions, *Quantum* **3**, 181 (2019).
- [64] E. M. Luks, F. Rákóczi, and C. R. Wright, Some algorithms for nilpotent permutation groups, *J. Symb. Comput.* **23**, 335 (1997).

CONTENTS

I. Introduction	1
II. Shadow estimation	2
III. Heisenberg-Weyl group and Clifford group	2
IV. Shadow estimation based on local Clifford measurements	2
V. Shadow estimation based on global Clifford measurements	3
VI. The power of magic gates in shadow estimation	4
VII. Numerical simulation	5
VIII. Summary	6
Acknowledgements	6
References	6
A. Proof of Eq. (2)	10
B. Qudit stabilizer formalism	10
1. Heisenberg-Weyl group and Clifford group	10
2. Stabilizer codes and stabilizer states	12
C. Proofs of Proposition 1 and Theorem 1	12
1. Auxiliary results	12
2. Proof of Proposition 1	13
3. Proof of Theorem 1	13
D. Magic gates and magic states	14
E. Proof sketches of Theorems 2-4	15
F. Additional numerical results	16
1. Shadow norms of stabilizer states and stabilizer projectors	16
2. Impacts of different T gates on shadow estimation	17
3. Simulation results on cluster states	17
4. Median of means estimation	18
G. Details of numerical simulation	19
1. Generating matrices of qudit stabilizer states	20
2. Tableau representation of qudit stabilizer states	21
3. Representation of qudit stabilizer states using Lagrangian subspaces and characteristic vectors	21
4. Simulation of stabilizer circuits	22
a. Tableau construction	22
b. Computational basis measurement	23
5. Simulation of Clifford circuits supplemented by T gates	24
a. Reverse gadgetization	24
b. Main simulation algorithm	25
c. Partial trace of stabilizer projectors	26

In this appendix, we prove Eq. (2), Proposition 1, and Theorem 1 and sketch the proofs of Theorems 2-4 based on our companion paper [46]. In addition, we develop a complete algorithm for simulating qudit shadow estimation based on the Clifford group supplemented by T gates and provide additional numerical results. Background on the qudit stabilizer formalism is also introduced for the convenience of the readers.

Appendix A: Proof of Eq. (2)

The MSE of the estimator \hat{o} only depends on the traceless part of \mathfrak{D} . To prove Eq. (2) we can assume that \mathfrak{D} is traceless without loss of generality; then $\mathfrak{D}_0 = \mathfrak{D}$. Suppose in the j th run the random unitary is U and the measurement outcome is \mathbf{b} . Then the corresponding single-shot estimator \hat{o}_j reads

$$\hat{o}_j := \text{tr}(\mathfrak{D}\hat{\rho}_j) = \text{tr}(\mathfrak{D}_0\hat{\rho}_j) = \text{tr}[\mathfrak{D}_0 \cdot \mathcal{M}^{-1}(U^\dagger|\mathbf{b}\rangle\langle\mathbf{b}|U)] = \text{tr}[\mathcal{M}^{-1}(\mathfrak{D}_0) \cdot U^\dagger|\mathbf{b}\rangle\langle\mathbf{b}|U], \quad (\text{A1})$$

where the last equality holds because the map \mathcal{M}^{-1} is self-adjoint. The expectation value of \hat{o}_j reads $\mathbb{E}[\hat{o}_j] = o = \text{tr}(\mathfrak{D}\rho) = \text{tr}(\mathfrak{D}_0\rho)$. So the variance of \hat{o}_j can be upper-bounded as follows,

$$\begin{aligned} \text{Var}[\hat{o}_j] &= \mathbb{E}[|\hat{o}_j - o|^2] \leq \mathbb{E}[|\hat{o}_j|^2] = \mathbb{E}\left[|\langle\mathbf{b}|U\mathcal{M}^{-1}(\mathfrak{D}_0)U^\dagger|\mathbf{b}\rangle|^2\right] \\ &= \mathbb{E}_{U \sim \mathcal{E}} \sum_{\mathbf{b} \in \mathbb{F}_d^n} \langle\mathbf{b}|U\rho U^\dagger|\mathbf{b}\rangle \cdot |\langle\mathbf{b}|U\mathcal{M}^{-1}(\mathfrak{D}_0)U^\dagger|\mathbf{b}\rangle|^2 \leq \|\mathfrak{D}_0\|_{\text{sh}}^2, \end{aligned} \quad (\text{A2})$$

where the last inequality follows from the definition of the shadow norm in Eq. (3). Note that this derivation is applicable even if \mathfrak{D} is not Hermitian.

By definition the empirical mean \hat{o} is the average of N independent single-shot estimators. Therefore,

$$\langle \varepsilon^2 \rangle = \text{Var}[\hat{o}] = \frac{1}{N^2} \sum_{j=1}^N \text{Var}[\hat{o}_j] \leq \frac{\|\mathfrak{D}_0\|_{\text{sh}}^2}{N}, \quad (\text{A3})$$

which confirms Eq. (2).

Appendix B: Qudit stabilizer formalism

In this appendix, we provide a bit more details on the qudit stabilizer formalism, assuming that the local dimension d is an odd prime.

1. Heisenberg-Weyl group and Clifford group

Recall that the HW group $\mathcal{W}(d)$ for a single qudit is generated by the two operators Z and X defined in Eq. (4), that is,

$$\mathcal{W}(d) := \langle Z, X \rangle = \{\omega_d^j Z^k X^l \mid j, k, l \in \mathbb{F}_d\}, \quad (\text{B1})$$

where $\omega_d = e^{\frac{2\pi i}{d}}$. Up to phase factors, the elements in $\mathcal{W}(d)$, known as Weyl operators, can be labeled by vectors in \mathbb{F}_d^2 [56]. Given $u = (p; q) \in \mathbb{F}_d^2$, define

$$W_u = W(p, q) := \chi(-pq/2)Z^p X^q, \quad (\text{B2})$$

where $\chi(r) = \omega_d^r$. Then $\mathcal{W}(d) = \{\omega_d^j W_u \mid j \in \mathbb{F}_d, u \in \mathbb{F}_d^2\}$. Let u, v be two vectors in \mathbb{F}_d^2 ; then W_u and W_v commute with each other iff u and v are linearly dependent.

The n -qudit HW group $\mathcal{W}(n, d)$ is the tensor product of n copies of $\mathcal{W}(d)$. Up to phase factors, the elements in $\mathcal{W}(n, d)$, known as n -qudit Weyl operators, can be labeled by column vectors in \mathbb{F}_d^{2n} . Given $\mathbf{u} = (u_1^z; u_2^z; \dots; u_n^z; u_1^x; u_2^x; \dots; u_n^x) \in \mathbb{F}_d^{2n}$, define

$$W_{\mathbf{u}} := W_{u_1} \otimes W_{u_2} \otimes \dots \otimes W_{u_n}, \quad (\text{B3})$$

where $u_j = (u_j^z; u_j^x)$. Then $\mathcal{W}(n, d) = \{\omega_d^j W_{\mathbf{u}} \mid j \in \mathbb{F}_d, \mathbf{u} \in \mathbb{F}_d^{2n}\}$. The weight of the Weyl operator $\omega_d^j W_{\mathbf{u}}$ is defined as the number of tensor factors in Eq. (B3) that are not equal to the identity operator I ; the Weyl operator is m local if it has weight m . Given $j, k \in \mathbb{F}_d$ and $\mathbf{u}, \mathbf{v} \in \mathbb{F}_d^{2n}$, the two Weyl operators $\omega_d^j W_{\mathbf{u}}$ and $\omega_d^k W_{\mathbf{v}}$ are locally commutative if W_{u_j} and W_{v_j} are commutative for $j = 1, 2, \dots, n$, where $v_j = (v_j^z; v_j^x)$.

To better understand the properties of the HW group, we need to introduce a symplectic structure in \mathbb{F}_d^{2n} . The symplectic product of \mathbf{u} and \mathbf{v} , denoted by $[\mathbf{u}, \mathbf{v}]$, is defined as follows,

$$[\mathbf{u}, \mathbf{v}] := \mathbf{u}^\top \Omega \mathbf{v}, \quad \Omega = \begin{pmatrix} 0_n & \mathbf{1}_n \\ -\mathbf{1}_n & 0_n \end{pmatrix}. \quad (\text{B4})$$

Then the composition and commutation relations of two Weyl operators $W_{\mathbf{u}}$ and $W_{\mathbf{v}}$ are determined by this symplectic product,

$$W_{\mathbf{u}}W_{\mathbf{v}} = \omega_d^{[\mathbf{u}, \mathbf{v}]/2} W_{\mathbf{u}+\mathbf{v}}, \quad W_{\mathbf{u}}W_{\mathbf{v}} = \omega_d^{[\mathbf{u}, \mathbf{v}]} W_{\mathbf{v}}W_{\mathbf{u}}, \quad \mathbf{u}, \mathbf{v} \in \mathbb{F}_d^{2n}. \quad (\text{B5})$$

In addition, this symplectic product defines the symplectic group $\text{Sp}(2n, d)$, which is composed of all $2n \times 2n$ matrices over \mathbb{F}_d that preserve the symplectic product, that is,

$$\text{Sp}(2n, d) := \{M \in \mathbb{F}_d^{2n \times 2n} \mid M^\top \Omega M = \Omega\}. \quad (\text{B6})$$

Elements in $\text{Sp}(2n, d)$ are called symplectic matrices or symplectic transformations. If M is a symplectic matrix, then $[M\mathbf{u}, M\mathbf{v}] = [\mathbf{u}, \mathbf{v}]$ for all $\mathbf{u}, \mathbf{v} \in \mathbb{F}_d^{2n}$.

To understand the structure of the symplectic group $\text{Sp}(2n, d)$. It is instructive to consider the following nested subgroup chain of symplectic groups,

$$G_1 \subset G_2 \subset \cdots \subset G_{n-1} \subset G_n = \text{Sp}(2n, d), \quad (\text{B7})$$

where G_m is a shorthand for $\text{Sp}(2m, d)$ for $m = 1, 2, \dots, n$, and the embedding $G_{m-1} \mapsto G_m$ is realized as follows,

$$M_{m-1} \mapsto \begin{pmatrix} 1 & 0 \\ 0 & 1 \end{pmatrix} \oplus M_{m-1}, \quad m = 2, 3, \dots, n, \quad M_{m-1} \in G_{m-1}. \quad (\text{B8})$$

Moreover, the map

$$\begin{aligned} G_n/G_{n-1} \times G_{n-1}/G_{n-2} \times \cdots \times G_2/G_1 \times G_1 &\rightarrow \text{Sp}(2n, d) \\ ([M_n], [M_{n-1}], \dots, [M_2], M_1) &\rightarrow M_n M_{n-1} \cdots M_2 M_1 \end{aligned} \quad (\text{B9})$$

is a bijection. Notably, each symplectic transformation $M \in \text{Sp}(2n, d)$ has a unique representation of the form $M_n M_{n-1} \cdots M_1$ with $[M_m] \in G_m/G_{m-1}$ for $m = 2, 3, \dots, n$ and $M_1 \in G_1$. This fact would come useful when sampling a random symplectic matrix or constructing a desired symplectic transformation.

The Clifford group $\text{Cl}(n, d)$ is the normalizer of the HW group $\mathcal{W}(n, d)$, that is,

$$\text{Cl}(n, d) := \{U \in \text{U}(\mathcal{H}_d^{\otimes n}) \mid U\mathcal{W}(n, d)U^\dagger = \mathcal{W}(n, d)\}, \quad (\text{B10})$$

where $\text{U}(\mathcal{H}_d^{\otimes n})$ is the group of unitary operators on $\mathcal{H}_d^{\otimes n}$. By definition the commutation relations of Weyl operators are invariant under Clifford transformations. So every Clifford unitary induces a symplectic transformation on the space \mathbb{F}_d^{2n} . Conversely, given any symplectic transformation $M \in \text{Sp}(2n, d)$, there exists a unitary operator $\mu(M)$ such that [56]

$$\mu(M)W_{\mathbf{u}}\mu(M)^\dagger = W_{M\mathbf{u}} \quad \forall \mathbf{u} \in \mathbb{F}_d^{2n}, \quad (\text{B11})$$

where μ is called the Weil or metaplectic representation of the symplectic group [57, 58]. Note that this conclusion relies on the assumption that d is an odd prime and does not hold when $d = 2$. Up to an overall phase factor, any Clifford unitary $C \in \text{Cl}(n, d)$ has the form

$$C = W_{\mathbf{a}}\mu(M), \quad \mathbf{a} \in \mathbb{F}_d^{2n}, \quad M \in \text{Sp}(2n, d). \quad (\text{B12})$$

In addition, we have

$$CW_{\mathbf{u}}C^\dagger = W_{\mathbf{a}}\mu(M)W_{\mathbf{u}}\mu(M)^\dagger W_{\mathbf{a}}^\dagger = W_{\mathbf{a}}W_{M\mathbf{u}}W_{\mathbf{a}}^\dagger = \chi([\mathbf{a}, M\mathbf{u}])W_{M\mathbf{u}}. \quad (\text{B13})$$

2. Stabilizer codes and stabilizer states

A subgroup \mathcal{S} of the HW group $\mathcal{W}(n, d)$ is a *stabilizer group* if it does not contain the operator $\omega_d \mathbb{I}$, in which case \mathcal{S} is automatically an elementary Abelian group and $|\mathcal{S}| \leq d^n$. Then the common eigenspace of \mathcal{S} with eigenvalue 1 defines a stabilizer code, denoted by $\mathcal{C}_{\mathcal{S}}$ hence forth. The projector onto $\mathcal{C}_{\mathcal{S}}$, known as a *stabilizer projector*, can be expressed as

$$P_{\mathcal{S}} = \frac{1}{|\mathcal{S}|} \sum_{U \in \mathcal{S}} U. \quad (\text{B14})$$

The dimension of the stabilizer code $\mathcal{C}_{\mathcal{S}}$ reads

$$\dim \mathcal{C}_{\mathcal{S}} = \text{rank } P_{\mathcal{S}} = \text{tr } P_{\mathcal{S}} = \frac{d^n}{|\mathcal{S}|}. \quad (\text{B15})$$

If \mathcal{S} can be generated by m Weyl operators, but cannot be generated by $m-1$ Weyl operators, then $|\mathcal{S}| = d^m$ and $\dim \mathcal{C}_{\mathcal{S}} = d^{n-m}$.

A stabilizer group \mathcal{S} in $\mathcal{W}(n, d)$ is maximal if it has the maximum order of d^n . In this case, the stabilizer code $\mathcal{C}_{\mathcal{S}}$ has dimension 1 and is determined by a normalized state, called a *stabilizer state*. A stabilizer state is uniquely determined by its stabilizer group, which is in turn determined by a generating set composed of n Weyl operators. The set of stabilizer states is denoted by $\text{Stab}(n, d)$, which is also regarded as a normalized ensemble. All stabilizer states in $\text{Stab}(n, d)$ form one orbit under the action of the Clifford group $\text{Cl}(n, d)$.

Appendix C: Proofs of Proposition 1 and Theorem 1

In this appendix, we prove Proposition 1 and Theorem 1, which clarify the shadow norms associated with local Clifford measurements. To this end, we need to introduce some auxiliary notation and results in preparation.

1. Auxiliary results

Let \mathbf{u}, \mathbf{v} be two vectors in \mathbb{F}_d^{2n} . The weight $|\mathbf{u}|$ of \mathbf{u} is defined as $|\mathbf{u}| := |\{j \mid (u_j^z; u_j^x) \neq (0; 0)\}|$. As a generalization, we define

$$\begin{aligned} |\mathbf{u} \vee \mathbf{v}| &:= |\{j \mid (u_j^z; u_j^x) \neq (0; 0) \text{ or } (v_j^z; v_j^x) \neq (0; 0)\}|, \\ |\mathbf{u} \wedge \mathbf{v}| &:= |\{j \mid (u_j^z; u_j^x) \neq (0; 0) \text{ and } (v_j^z; v_j^x) \neq (0; 0)\}|. \end{aligned} \quad (\text{C1})$$

Evidently, we have

$$|\mathbf{u} \vee \mathbf{v}| + |\mathbf{u} \wedge \mathbf{v}| = |\mathbf{u}| + |\mathbf{v}|. \quad (\text{C2})$$

Next, we introduce two relations on \mathbb{F}_d^{2n} . We write $\mathbf{u} \triangleright \mathbf{v}$ if u_j is proportional to v_j for $j = 1, 2, \dots, n$ and write $\mathbf{u} \bowtie \mathbf{v}$ if u_j, v_j are linearly dependent for $j = 1, 2, \dots, n$. In this case, we can deduce the following relations,

$$|\mathbf{u} \vee \mathbf{v}| = \min\{|\mathbf{s}| : \mathbf{s} \in \mathbb{F}_d^{2n}, \mathbf{u} \triangleright \mathbf{s}, \mathbf{v} \triangleright \mathbf{s}\}, \quad |\mathbf{u} \wedge \mathbf{v}| = \max\{|\mathbf{s}| : \mathbf{s} \in \mathbb{F}_d^{2n}, \mathbf{s} \triangleright \mathbf{u}, \mathbf{s} \triangleright \mathbf{v}\}. \quad (\text{C3})$$

If $\mathbf{u} \triangleright \mathbf{v}$, then $\mathbf{u} \bowtie \mathbf{v}$, but the converse is not guaranteed in general. Let $j, k \in \mathbb{F}_d$. Then the Weyl operator $\omega_d^j W_{\mathbf{u}}$ is m local iff $|\mathbf{u}| = m$. The two Weyl operators $\omega_d^j W_{\mathbf{u}}$ and $\omega_d^k W_{\mathbf{v}}$ are locally commutative iff $\mathbf{u} \bowtie \mathbf{v}$.

Lemma 1. *Suppose d is an odd prime, $\mathbf{b} \in \mathbb{F}_d^n$, and $\mathbf{u}, \mathbf{v} \in \mathbb{F}_d^{2n}$. Then we have*

$$\mathbb{E}_{U \sim \text{Cl}(d)^{\otimes n}} (U^\dagger |\mathbf{b}\rangle \langle \mathbf{b}| U \langle \mathbf{b}| U W_{\mathbf{u}} U^\dagger |\mathbf{b}\rangle \langle \mathbf{b}| U W_{\mathbf{v}} U^\dagger |\mathbf{b}\rangle \langle \mathbf{b}|) = \begin{cases} d^{-n} (d+1)^{-|\mathbf{u} \vee \mathbf{v}|} W_{\mathbf{u}} W_{\mathbf{v}}^\dagger & \text{if } \mathbf{u} \bowtie \mathbf{v}, \\ 0 & \text{otherwise.} \end{cases} \quad (\text{C4})$$

Proof. Thanks to the tensor structure of U , $W_{\mathbf{u}}$, $W_{\mathbf{v}}$, and $|\mathbf{b}\rangle$, it suffices to prove Eq. (C4) in the case $n = 1$. Then we can rewrite the LHS of Eq. (C4) as follows,

$$\mathbb{E}_{|\Psi\rangle \sim \text{Stab}(d)} (|\Psi\rangle \langle \Psi| \langle \Psi| W_{\mathbf{u}} |\Psi\rangle \langle \Psi| W_{\mathbf{v}} |\Psi\rangle \langle \Psi|) = \frac{1}{d(d+1)} \sum_{|\Psi\rangle \in \text{Stab}(d)} (|\Psi\rangle \langle \Psi| \langle \Psi| W_{\mathbf{u}} |\Psi\rangle \langle \Psi| W_{\mathbf{v}} |\Psi\rangle \langle \Psi|), \quad (\text{C5})$$

where $\text{Stab}(d)$ is the set of single-qudit stabilizer states. If $W_{\mathbf{u}}$ and $W_{\mathbf{v}}$ do not commute, then they cannot belong to the stabilizer group of any stabilizer state simultaneously. Therefore, $\langle \Psi | W_{\mathbf{u}} | \Psi \rangle \langle \Psi | W_{\mathbf{v}} | \Psi \rangle^* = 0$, which implies Eq. (C4). If $W_{\mathbf{u}} = W_{\mathbf{v}} = \mathbb{I}$, then Eq. (C4) holds because $\mathbb{E}_{|\Psi\rangle \sim \text{Stab}(d)} |\Psi\rangle \langle \Psi| = \mathbb{I}/d$.

Next, suppose $W_{\mathbf{u}}$ and $W_{\mathbf{v}}$ commute, and at least one of them is not proportional to the identity operator. Then we can find a Clifford unitary $C \in \text{Cl}(d)$ such that

$$C^\dagger W_{\mathbf{u}} C = \omega_d^{r_1} Z^{s_1}, \quad C^\dagger W_{\mathbf{v}} C = \omega_d^{r_2} Z^{s_2}, \quad (\text{C6})$$

where $r_1, s_1, r_2, s_2 \in \mathbb{F}_d$. Therefore,

$$\begin{aligned} & \sum_{|\Psi\rangle \in \text{Stab}(d)} (|\Psi\rangle \langle \Psi| \langle \Psi | W_{\mathbf{u}} | \Psi \rangle \langle \Psi | W_{\mathbf{v}} | \Psi \rangle^*) = \sum_{|\Psi\rangle \in \text{Stab}(d)} (|\Psi\rangle \langle \Psi| \langle \Psi | C \omega_d^{r_1} Z^{s_1} C^\dagger | \Psi \rangle \langle \Psi | C \omega_d^{r_2} Z^{s_2} C^\dagger | \Psi \rangle^*) \\ &= \sum_{|\Psi\rangle \in \text{Stab}(d)} (C |\Psi\rangle \langle \Psi| C^\dagger \langle \Psi | \omega_d^{r_1} Z^{s_1} | \Psi \rangle \langle \Psi | \omega_d^{r_2} Z^{s_2} | \Psi \rangle^*) = \sum_{b \in \mathbb{F}_d} (C |b\rangle \langle b| C^\dagger \langle b | \omega_d^{r_1} Z^{s_1} | b \rangle \langle b | \omega_d^{r_2} Z^{s_2} | b \rangle^*) \\ &= C \omega_d^{r_1} Z^{s_1} \omega_d^{-r_2} Z^{-s_2} C^\dagger = W_{\mathbf{u}} W_{\mathbf{v}}^\dagger. \end{aligned} \quad (\text{C7})$$

Together with Eq. (C5), this equation implies Eq. (C4) and completes the proof of Lemma 1. \square

For local Clifford measurements, the reconstruction map \mathcal{M}^{-1} in Eq. (5) can be expressed as

$$\mathcal{M}^{-1} = \left(\mathcal{D}_{1/(d+1)}^{-1} \right)^{\otimes n}, \quad (\text{C8})$$

where $\mathcal{D}_y^{-1}(\cdot)$ is the inverse of the single-qudit depolarizing channel $\mathcal{D}_y(\cdot) = y \cdot + (1-y) \frac{\text{tr}(\cdot)}{d} I$. Note that $\mathcal{D}_{1/(d+1)}^{-1}(\mathfrak{D}) = (d+1)\mathfrak{D} - \text{tr}(\mathfrak{D})I$ for any linear operator \mathfrak{D} on \mathcal{H}_d . If $\mathfrak{D} = W_u$ is a Weyl operator with $u \in \mathbb{F}_d^2$, then

$$\mathcal{D}_{1/(d+1)}^{-1}(W_u) = \begin{cases} W_u & \text{if } W_u \propto I, \\ (d+1)W_u & \text{otherwise.} \end{cases} \quad (\text{C9})$$

2. Proof of Proposition 1

Proof of Proposition 1. If $d = 2$, then Proposition 1 holds according to Lemma 3 in Ref. [1].

Next, suppose d is an odd prime and \mathfrak{D} is an m -local Weyl operator. Then \mathfrak{D} has the form $\mathfrak{D} = e^{i\phi} W_{\mathbf{u}}$, where ϕ is a real phase and $\mathbf{u} \in \mathbb{F}_d^{2m}$ with $|\mathbf{u}| = m$. By virtue of Eqs. (3) and (C8) we can deduce that

$$\begin{aligned} \|\mathfrak{D}\|_{\text{sh}}^2 &= \|W_{\mathbf{u}}\|_{\text{sh}}^2 = \max_{\sigma} \sum_{\mathbf{b} \in \mathbb{F}_d^n} \mathbb{E}_{U \sim \text{Cl}(d)^{\otimes n}} \left[\langle \mathbf{b} | U \sigma U^\dagger | \mathbf{b} \rangle \cdot \left| \langle \mathbf{b} | U \left(\mathcal{D}_{1/(d+1)}^{-1} \right)^{\otimes n} (W_{\mathbf{u}}) U^\dagger | \mathbf{b} \rangle \right|^2 \right] \\ &= (d+1)^{2m} \max_{\sigma} \sum_{\mathbf{b} \in \mathbb{F}_d^n} \mathbb{E}_{U \sim \text{Cl}(d)^{\otimes n}} \left[\langle \mathbf{b} | U \sigma U^\dagger | \mathbf{b} \rangle \cdot \left| \langle \mathbf{b} | U W_{\mathbf{u}} U^\dagger | \mathbf{b} \rangle \right|^2 \right] \\ &= d^n (d+1)^{2m} \times \frac{1}{d^n (d+1)^m} \max_{\sigma} \text{tr}(\sigma W_{\mathbf{u}} W_{\mathbf{u}}^\dagger) = (d+1)^m, \end{aligned} \quad (\text{C10})$$

which confirms Proposition 1. Here the second equality follows from Eq. (C9) and the fact that $W_{\mathbf{u}}$ is m -local, and the last equality follows from Lemma 1. \square

3. Proof of Theorem 1

Proof of Theorem 1. If $d = 2$, then Eq. (7) follows from Proposition 3 in Ref. [1], so it remains to consider the case in which d is an odd prime.

We expand $\tilde{\mathfrak{D}}$ in the Weyl basis as $\tilde{\mathfrak{D}} = \sum_{\mathbf{u} \in \mathbb{F}_d^{2m}} \alpha_{\mathbf{u}} W_{\mathbf{u}}$. According to Eq. (C9), we have

$$\left(\mathcal{D}_{1/(d+1)}^{-1} \right)^{\otimes m} (\tilde{\mathfrak{D}}) = \sum_{\mathbf{u} \in \mathbb{F}_d^{2m}} (d+1)^{|\mathbf{u}|} \alpha_{\mathbf{u}} W_{\mathbf{u}}. \quad (\text{C11})$$

Define $\mathcal{V}_1^* \subset \mathbb{F}_d^2$ and $\mathcal{V}_m^* \subset \mathbb{F}_d^{2m}$ as follows,

$$\begin{aligned}\mathcal{V}_1^* &:= \{(0; 1), (1; 1), \dots, (d-1; 1), (1; 0)\}, \\ \mathcal{V}_m^* &:= \{(s_{z,1}; s_{z,2}; \dots; s_{z,m}; s_{x,1}; s_{x,2}; \dots; s_{x,m}) \mid (s_j^z; s_j^x) \in \mathcal{V}_1^*, \forall 1 \leq j \leq m\}.\end{aligned}\quad (\text{C12})$$

In conjunction with Eqs. (3) and (C8) we can deduce that

$$\begin{aligned}\|\mathcal{D}\|_{\text{sh}}^2 &= \|\tilde{\mathcal{D}}\|_{\text{sh}}^2 = \max_{\sigma} \mathbb{E}_{U \sim \text{Cl}(d)^{\otimes m}} \sum_{\mathbf{b} \in \mathbb{F}_d^m} \left[\langle \mathbf{b} | U \sigma U^\dagger | \mathbf{b} \rangle \left| \langle \mathbf{b} | U \left(\mathcal{D}_{1/(d+1)}^{-1} \right)^{\otimes m} (\tilde{\mathcal{D}}) U^\dagger | \mathbf{b} \rangle \right|^2 \right] \\ &= \max_{\sigma} \sum_{\mathbf{b} \in \mathbb{F}_d^m} \sum_{\mathbf{u}, \mathbf{v} \in \mathbb{F}_d^{2m}} \left\{ (d+1)^{|\mathbf{u}|+|\mathbf{v}|} \alpha_{\mathbf{u}} \alpha_{\mathbf{v}}^* \text{tr} [\sigma \cdot \mathbb{E}_{U \sim \text{Cl}(d)^{\otimes m}} U^\dagger | \mathbf{b} \rangle \langle \mathbf{b} | U \langle \mathbf{b} | U W_{\mathbf{u}} U^\dagger | \mathbf{b} \rangle \langle \mathbf{b} | U W_{\mathbf{v}} U^\dagger | \mathbf{b} \rangle^*] \right\} \\ &= \max_{\sigma} \sum_{\mathbf{u}, \mathbf{v} \in \mathbb{F}_d^{2m}, \mathbf{u} \triangleright \mathbf{v}} \left[\frac{(d+1)^{|\mathbf{u}|+|\mathbf{v}|}}{(d+1)^{|\mathbf{u}\mathbf{v}\mathbf{v}|}} \alpha_{\mathbf{u}} \alpha_{\mathbf{v}}^* \text{tr} (\sigma W_{\mathbf{u}} W_{\mathbf{v}}^\dagger) \right] = \left\| \sum_{\mathbf{u}, \mathbf{v} \in \mathbb{F}_d^{2m}, \mathbf{u} \triangleright \mathbf{v}} \frac{(d+1)^{|\mathbf{u}|+|\mathbf{v}|}}{(d+1)^{|\mathbf{u}\mathbf{v}\mathbf{v}|}} \alpha_{\mathbf{u}} \alpha_{\mathbf{v}}^* W_{\mathbf{u}} W_{\mathbf{v}}^\dagger \right\| \\ &= \left\| \sum_{\mathbf{s} \in \mathcal{V}_m^*} \sum_{\mathbf{u}, \mathbf{v} \triangleright \mathbf{s}} \frac{(d+1)^{|\mathbf{u}|+|\mathbf{v}|}}{(d+1)^m} \alpha_{\mathbf{u}} \alpha_{\mathbf{v}}^* W_{\mathbf{u}} W_{\mathbf{v}}^\dagger \right\| \leq \frac{1}{(d+1)^m} \sum_{\mathbf{s} \in \mathcal{V}_m^*} \left\| \sum_{\mathbf{u}, \mathbf{v} \triangleright \mathbf{s}} (d+1)^{|\mathbf{u}|+|\mathbf{v}|} \alpha_{\mathbf{u}} \alpha_{\mathbf{v}}^* W_{\mathbf{u}} W_{\mathbf{v}}^\dagger \right\| \\ &= \frac{1}{(d+1)^m} \sum_{\mathbf{s} \in \mathcal{V}_m^*} \left\| \sum_{\mathbf{u} \triangleright \mathbf{s}} (d+1)^{|\mathbf{u}|} \alpha_{\mathbf{u}} W_{\mathbf{u}} \right\|^2 \leq \frac{1}{(d+1)^m} \sum_{\mathbf{s} \in \mathcal{V}_m^*} \left| \sum_{\mathbf{u} \triangleright \mathbf{s}} (d+1)^{|\mathbf{u}|} \alpha_{\mathbf{u}} \right|^2,\end{aligned}\quad (\text{C13})$$

where each maximization is over all quantum states on $\mathcal{H}_d^{\otimes n}$. Here the fourth equality follows from Lemma 1 and the sixth equality holds because

$$|\{\mathbf{s} \in \mathcal{V}_m^* \mid \mathbf{u}, \mathbf{v} \triangleright \mathbf{s}\}| = (d+1)^{m-|\mathbf{u}\mathbf{v}\mathbf{v}|}.\quad (\text{C14})$$

When $\tilde{\mathcal{D}} = W_{\mathbf{q}}$ is an m -local Weyl operator, say, $\tilde{\mathcal{D}} = W_{\mathbf{q}}$ with $\mathbf{q} \in \mathbb{F}_d^{2m}$ and $|\mathbf{q}| = m$, we have $\alpha_{\mathbf{u}} = 1$ if $\mathbf{u} = \mathbf{q}$ and $\alpha_{\mathbf{u}} = 0$ otherwise, so both inequalities in Eq. (C13) are saturated and we recover Proposition 1.

Next, by virtue of the Cauchy-Schwartz inequality applied to Eq. (C13) we can deduce that

$$\begin{aligned}\|\mathcal{D}\|_{\text{sh}}^2 &\leq \frac{1}{(d+1)^m} \sum_{\mathbf{s} \in \mathcal{V}_m^*} \left| \sum_{\mathbf{u} \triangleright \mathbf{s}} (d+1)^{|\mathbf{u}|} \alpha_{\mathbf{u}} \right|^2 \leq \frac{1}{(d+1)^m} \sum_{\mathbf{s} \in \mathcal{V}_m^*} \left(\sum_{\mathbf{u} \triangleright \mathbf{s}} (d+1)^{|\mathbf{u}|} \right) \left(\sum_{\mathbf{u} \triangleright \mathbf{s}} (d+1)^{|\mathbf{u}|} |\alpha_{\mathbf{u}}|^2 \right) \\ &= d^{2m} \sum_{\mathbf{s} \in \mathcal{V}_m^*} \sum_{\mathbf{u} \triangleright \mathbf{s}} (d+1)^{|\mathbf{u}|-m} |\alpha_{\mathbf{u}}|^2 = d^{2m} \sum_{\mathbf{u} \in \mathbb{F}_d^{2m}} |\alpha_{\mathbf{u}}|^2 = d^m \|\tilde{\mathcal{D}}\|_2^2,\end{aligned}\quad (\text{C15})$$

which confirms Theorem 1. In deriving the above equalities we have taken into account the following facts,

$$\sum_{\mathbf{u} \triangleright \mathbf{s}} (d+1)^{|\mathbf{u}|} = \sum_{j=0}^m \binom{m}{j} (d-1)^j (d+1)^j = d^{2m}, \quad |\{\mathbf{s} \in \mathcal{V}_m^* \mid \mathbf{u} \triangleright \mathbf{s}\}| = (d+1)^{m-|\mathbf{u}|}.\quad (\text{C16})$$

□

Appendix D: Magic gates and magic states

Recall that a qudit T gate is a diagonal magic gate within the third Clifford hierarchy [46, 49]. It is determined by a cubic function as shown in Eq. (13). For each T gate on \mathcal{H}_d we can define a magic state as follows,

$$|T\rangle := TF|0\rangle = T|+\rangle,\quad (\text{D1})$$

where $|+\rangle := F|0\rangle = \sum_{u \in \mathbb{F}_d} |u\rangle / \sqrt{d}$. By definition, $|T\rangle$ can be generated from $|0\rangle$ by the magic gate T following the Fourier gate F . In addition, the conjugate T^\dagger is also a diagonal magic gate and the corresponding magic state reads

$$|T^\dagger\rangle = T^\dagger F|0\rangle = T^\dagger F^\dagger|0\rangle,\quad (\text{D2})$$

TABLE I. Specific choices of primitive elements for \mathbb{F}_d with $d < 50$.

d	3	5	7	11	13	17	19	23	29	31	37	41	43	47
ν	2	2	3	2	2	3	2	5	2	3	2	6	3	5

where the second inequality holds because $F|0\rangle = F^\dagger|0\rangle = |+\rangle$.

When $d \equiv 1 \pmod{3}$, each T gate is determined by a cubit polynomial f over \mathbb{F}_d . We can distinguish three types of T gates depending on the cubic coefficient c ($c \neq 0$ by definition) of the underlying cubic polynomial f [46]. More precisely, T gates are distinguished by cubic characters of cubic coefficients. Let ν be a given primitive element of the field \mathbb{F}_d ; see Table I for specific choices when $d < 50$. Let η_3 be the cubic character on $\mathbb{F}_d^\times := \mathbb{F}_d \setminus \{0\}$ defined as follows,

$$\eta_3(\nu^j) := \omega_3^j, \quad j = 0, 1, \dots, d-2, \quad (\text{D3})$$

where $\omega_3 = e^{2\pi i/3}$. The cubic character of T is defined as the cubic character of the cubic coefficient c , that is, $\eta_3(T) = \eta_3(c)$. Note that $\eta_3(T) = 1$ iff the cubic coefficient c is a cubic residue, that is, a cube of another element in \mathbb{F}_d^\times . For example, we have $\eta_3(T) = 1$ when $c = 1$, which is the case for the canonical T gate. It turns out different types of T gates have different performances in shadow estimation; see Appendix F 2 and the companion paper [46] for more details. In other words, we can improve the performance by educated choices of T gates. Incidentally, when $d = 3$ or $d \equiv 2 \pmod{3}$, all T gates have the same performance, so it is not necessary to distinguish different T gates.

Appendix E: Proof sketches of Theorems 2-4

In this section we sketch the proofs of Theorems 2-4 based on our companion paper [46].

Suppose the unitary ensemble \mathcal{E} used in shadow estimation forms a unitary 2-design. Denote by $Q(\mathcal{E})$ and $\bar{Q}(\mathcal{E})$ the third moment operator and normalized moment operator associated with the corresponding measurement ensemble, that is,

$$Q(\mathcal{E}) := \frac{1}{D} \mathbb{E}_{U \sim \mathcal{E}} \sum_{\mathbf{b} \in \mathbb{F}_d^n} (U^\dagger |\mathbf{b}\rangle \langle \mathbf{b}| U)^{\otimes 3}, \quad (\text{E1})$$

$$\bar{Q}(\mathcal{E}) := \frac{D(D+1)(D+2)}{6} Q(\mathcal{E}) = \frac{(D+1)(D+2)}{6} \mathbb{E}_{U \sim \mathcal{E}} \sum_{\mathbf{b} \in \mathbb{F}_d^n} (U^\dagger |\mathbf{b}\rangle \langle \mathbf{b}| U)^{\otimes 3}, \quad (\text{E2})$$

which are Hermitian operators on $\mathcal{H}^{\otimes 3}$. For the convenience of the following discussion, we label the three copies of \mathcal{H} by A, B, C , respectively. Then the shadow norm in Eq. (3) can be expressed as follows,

$$\begin{aligned} \|\mathfrak{D}\|_{\text{sh}}^2 &= \max_{\sigma} \mathbb{E}_{U \sim \mathcal{E}} \sum_{\mathbf{b} \in \mathbb{F}_d^n} \left[\langle \mathbf{b}| U \sigma U^\dagger |\mathbf{b}\rangle \cdot |\langle \mathbf{b}| U \mathcal{M}^{-1}(\mathfrak{D}) U^\dagger |\mathbf{b}\rangle|^2 \right] = \max_{\sigma} D \text{tr} [Q(\mathcal{E})(\sigma \otimes \mathcal{M}^{-1}(\mathfrak{D}) \otimes \mathcal{M}^{-1}(\mathfrak{D})^\dagger)] \\ &= \max_{\sigma} D(D+1)^2 \text{tr} [Q(\mathcal{E})(\sigma \otimes \mathfrak{D} \otimes \mathfrak{D}^\dagger)] = \max_{\sigma} \frac{6(D+1)}{D+2} \text{tr} [\bar{Q}(\mathcal{E})(\sigma \otimes \mathfrak{D} \otimes \mathfrak{D}^\dagger)] \\ &= \frac{6(D+1)}{D+2} \|\text{tr}_{BC} [\bar{Q}(\mathcal{E})(I \otimes \mathfrak{D} \otimes \mathfrak{D}^\dagger)]\| \end{aligned} \quad (\text{E3})$$

where the third equality holds because $\mathcal{M}^{-1}(\mathfrak{D}) = (D+1)\mathfrak{D}$ given that \mathcal{E} is a 2-design and \mathfrak{D} is traceless. The above expression for the shadow norm has the same form as in Eq. (14) in our companion paper [46].

Next, we turn to shadow estimation based on the Clifford group supplemented by T gates, in which case the moment operator $Q(\mathcal{E})$ is identical to the moment operator of a suitable Clifford orbit, as we shall see shortly.

Lemma 2. *Suppose $\mathcal{E} = \text{Cl}(n, d)$; then*

$$Q(\mathcal{E}) = \mathbb{E}_{U \sim \mathcal{E}} (U^\dagger |\mathbf{0}\rangle \langle \mathbf{0}| U)^{\otimes 3}, \quad (\text{E4})$$

where $|\mathbf{0}\rangle$ is a shorthand for $|0\rangle^{\otimes n}$.

Lemma 3. Suppose $\mathcal{E} = \mathcal{E}(\{T_j\}_{j=1}^k)$ and $|\Psi\rangle = |T_1^\dagger\rangle \otimes \cdots \otimes |T_k^\dagger\rangle \otimes |0\rangle^{\otimes(n-k)}$, where $|T_j^\dagger\rangle$ for $j = 1, 2, \dots, k$ are defined according to Eq. (D2). Then

$$Q(\mathcal{E}) = \mathbb{E}_{U \sim \text{Cl}(n,d)} (U^\dagger |\Psi\rangle \langle \Psi| U)^{\otimes 3}. \quad (\text{E5})$$

Lemma 2 shows that the moment operator $Q(\mathcal{E})$ associated with the Clifford ensemble is identical to the counterpart of the orbit $\text{Stab}(n, d)$ of stabilizer states (and similarly for the normalized moment operator). This result is expected given that all computational basis states form one orbit under the action of the Clifford group. It highlights the importance of the moment operator in studying shadow estimation. The key properties of the moment operator of $\text{Stab}(n, d)$ have been clarified in our companion paper [46] after systematic and in-depth study. Thanks to Lemma 2, Theorems 2 and 3 follow from Theorems 4 and 3 in the companion paper, respectively. Lemma 3 further shows that the moment operator $Q(\mathcal{E})$ associated with the ensemble $\mathcal{E} = \mathcal{E}(\{T_j\}_{j=1}^k)$ is identical to the moment operator of a Clifford orbit generated from a magic state. Therefore, Theorem 4 follows from Theorems 15 and 21 in the companion paper [46].

In the following proof we use $X^{\mathbf{b}}$ as a shorthand for $X^{b_1} \otimes \cdots \otimes X^{b_n}$.

Proof of Lemma 2. By virtue of the definition in Eq. (E1) we can deduce that

$$Q(\mathcal{E}) = \frac{1}{D} \mathbb{E}_{U \sim \mathcal{E}} \sum_{\mathbf{b} \in \mathbb{F}_d^n} (U^\dagger |\mathbf{b}\rangle \langle \mathbf{b}| U)^{\otimes 3} = \frac{1}{D} \mathbb{E}_{U \sim \mathcal{E}} \sum_{\mathbf{b} \in \mathbb{F}_d^n} (U^\dagger X^{\mathbf{b}} |\mathbf{0}\rangle \langle \mathbf{0}| X^{-\mathbf{b}} U)^{\otimes 3} = \mathbb{E}_{U \sim \mathcal{E}} (U^\dagger |\mathbf{0}\rangle \langle \mathbf{0}| U)^{\otimes 3}, \quad (\text{E6})$$

which confirms Eq. (E4). Here the second equality holds because $|\mathbf{b}\rangle = X^{\mathbf{b}} |\mathbf{0}\rangle$, and the third equality holds because $X^{\mathbf{b}} \in \text{Cl}(n, d)$. \square

Proof of Lemma 3. Let $V = FT_1 \otimes \cdots \otimes FT_k \otimes I^{\otimes(n-k)}$. Then

$$|\Psi\rangle = V^\dagger |\mathbf{0}\rangle, \quad V^\dagger X^{\mathbf{b}} = V^\dagger X^{\mathbf{b}} V V^\dagger = (Z^{-b_1} \otimes \cdots \otimes Z^{-b_k} \otimes X^{b_{k+1}} \otimes \cdots \otimes X^{b_n}) V^\dagger, \quad (\text{E7})$$

where the third equality holds because $T_j^\dagger F^\dagger X F T_j = T_j^\dagger Z^{-1} T_j = Z^{-1}$ for $j = 1, 2, \dots, k$. In addition, $\mathcal{E} = \mathcal{E}(\{T_j\}_{j=1}^k) = V \text{Cl}(n, d)$ and

$$\begin{aligned} Q(\mathcal{E}) &= \frac{1}{D} \mathbb{E}_{U \sim \mathcal{E}} \sum_{\mathbf{b} \in \mathbb{F}_d^n} (U^\dagger |\mathbf{b}\rangle \langle \mathbf{b}| U)^{\otimes 3} = \frac{1}{D} \mathbb{E}_{U \sim \text{Cl}(n,d)} \sum_{\mathbf{b} \in \mathbb{F}_d^n} (U^\dagger V^\dagger X^{\mathbf{b}} |\mathbf{0}\rangle \langle \mathbf{0}| X^{-\mathbf{b}} V U)^{\otimes 3} \\ &= \frac{1}{D} \mathbb{E}_{U \sim \text{Cl}(n,d)} \sum_{\mathbf{b} \in \mathbb{F}_d^n} (U_{\mathbf{b}}^\dagger |\Psi\rangle \langle \Psi| U_{\mathbf{b}})^{\otimes 3} = \mathbb{E}_{U \sim \text{Cl}(n,d)} (U^\dagger |\Psi\rangle \langle \Psi| U)^{\otimes 3}, \end{aligned} \quad (\text{E8})$$

where $U_{\mathbf{b}} = (Z^{b_1} \otimes \cdots \otimes Z^{b_k} \otimes X^{-b_{k+1}} \otimes \cdots \otimes X^{-b_n}) U$ and the third equality follows from Eq. (E7). This equation confirms Eq. (E5) and completes the proof of Lemma 3. \square

Appendix F: Additional numerical results

1. Shadow norms of stabilizer states and stabilizer projectors

In the main text we have shown that, compared with the qubit case, the overhead in qudit shadow estimation based on the Clifford group is almost independent of the qudit number n . Moreover, this overhead vanishes exponentially with the increase of T gates; actually, a single T gate can already suppress the overhead to a constant factor that is independent of the local dimension, as illustrated in Fig. 1. Here we provide some additional results on the shadow norms associated with stabilizer states and stabilizer projectors. Figure 6 shows the (squared) shadow norm associated with the projector \mathfrak{D} onto an n -qudit stabilizer state as a function of the local dimension d and the number k of canonical T gates. The deviation $\|\mathfrak{D}_0\|_{\text{sh}}^2 - 3$ decreases exponentially with k , and it tends to decrease more quickly as the local dimension increases, which agrees with Theorem 4. Note that \mathfrak{D}_0 denotes the traceless part of \mathfrak{D} and $\|\mathfrak{D}_0\|_{\text{sh}}^2 \approx 3$ if the measurement primitive is a 3-design, which is the case in the qubit setting. Therefore, the Clifford circuit supplemented by a few T gates can achieve almost the same performance as 3-design ensembles. Figure 7 further shows the shadow norms associated with normalized stabilizer projectors.

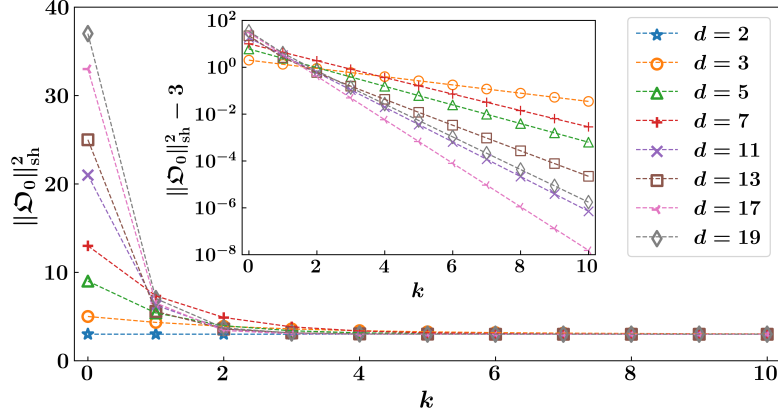


FIG. 6. Squared shadow norm associated with the projector \mathcal{D} onto an n -qudit stabilizer state with respect to the Clifford circuit supplemented by k canonical T gates. Here $n = 50$ and \mathcal{D}_0 denotes the traceless part of \mathcal{D} .

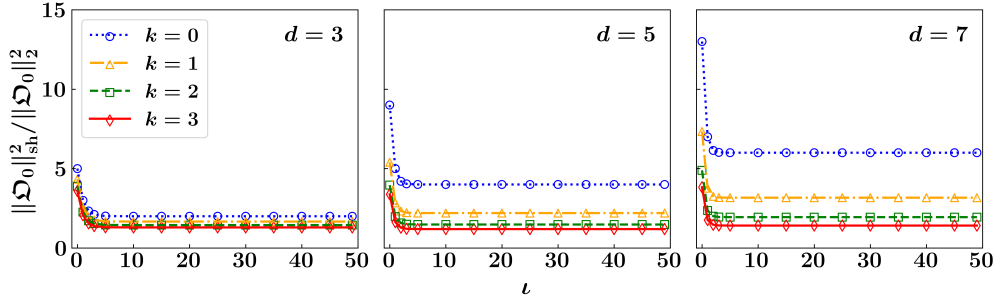


FIG. 7. The ratio between the squared shadow norm $\|\mathcal{D}_0\|_{\text{sh}}^2$ and squared Hilbert-Schmidt norm $\|\mathcal{D}_0\|_2^2$. Here \mathcal{D} is an n -qudit rank- K stabilizer projector with $n = 50$, $K = d^t$, and $\|\mathcal{D}_0\|_2^2 = K - K^2/D$. The unitary ensemble is based on the Clifford circuit supplemented by k canonical T gates.

2. Impacts of different T gates on shadow estimation

When $d = 1 \pmod 3$, we can distinguish three types of T gates depending on the cubic characters of cubic coefficients of the underlying cubic polynomials as mentioned in Appendix D and discussed in more details in our companion paper [46]. Here we illustrate the impacts of different T gates on the performance in shadow estimation. Table II lists the optimal choices of one and two T gates in fidelity estimation of n -qudit stabilizer states with $n = 100$ and $d = 7, 13, 19, 31$. Figure 8 illustrates the significant impacts of different T gates on the shadow norms of random two-qudit traceless (diagonal) observables and on the MSE in fidelity estimation of the 100-qudit GHZ state with $d = 7$. The optimal choices of one and two T gates are consistent with the results in Table II.

3. Simulation results on cluster states

Here we provide additional simulation results on fidelity estimation of cluster states based on the Clifford circuit supplemented by up to two canonical T gates. Figure 9 shows the inverse MSE in estimating the fidelity of the 100-qudit cluster state defined on a 10×10 square lattice with periodic boundary condition. The overall behavior is similar to the counterpart of the GHZ state as shown in Fig. 4.

TABLE II. Optimal choices of one and two T gates (in minimizing the shadow norms) in fidelity estimation of n -qudit stabilizer states with $n = 100$ and $d = 7, 13, 19, 31$. Here ν is a primitive element in the finite field \mathbb{F}_d (cf. Table I). Different T gates are distinguished by cubic coefficients of the underlying cubic polynomials expressed as powers of ν ; exponents of ν are distinguished only modulo 3.

d	ν	T	$2T$ (identical)	$2T$
7	3	$[\nu^2]$	$[\nu^2, \nu^2]$	$[\nu, \nu^2]$
13	2	$[1]$	$[1, 1]$	$[1, \nu]$
19	2	$[\nu^2]$	$[\nu^2, \nu^2]$	$[1, \nu^2]$
31	3	$[1]$	$[1, 1]$	$[1, \nu^2]$

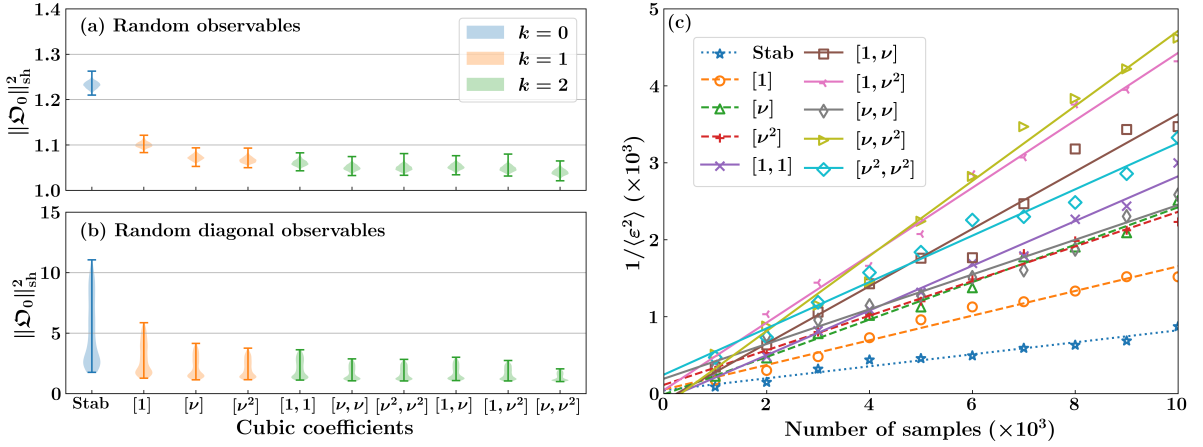


FIG. 8. Impacts of different T gates on shadow estimation in the case $d = 7$. Here the unitary ensemble \mathcal{E} is based on the Clifford circuit supplemented by k T gates. The special case $k = 0$ is labeled by ‘Stab’ because the corresponding measurement primitive is $\text{Stab}(n, d)$; when $k = 1, 2$, different T gates are distinguished by cubic coefficients as in Table II with $\nu = 3$. (a,b) Distributions of the shadow norms of random two-qudit traceless (diagonal) observables that are normalized with respect to the Hilbert-Schmidt norm. (c) Simulation results on the inverse MSE in estimating the fidelity of the 100-qudit GHZ state. The MSE $\langle \varepsilon^2 \rangle$ for each data point is the average over 100 runs. Here the dotted, dashed, and solid lines correspond to the cases with $k = 0, 1, 2$, respectively; they are determined by interpolation.

4. Median of means estimation

So far the estimator employed in our numerical simulation is based on the empirical mean in Eq. (1). As an alternative, we can also employ the median of means [1]. To this end, we first divide the N samples into L groups, each containing N/L samples, assuming that N is a multiple of L . For each group we can construct an estimator based on the empirical mean. In this way, we can construct L preliminary estimators. Now, the final estimator is the median of the L preliminary estimators. Compared with the estimator in Eq. (1), this alternative estimator can effectively reduce the probability of large deviation at the prize of a slightly larger MSE.

Figure 10 illustrates the performance of this estimator with $L = 10$ in estimating the fidelity of the 100-qudit GHZ state based on the qudit Clifford group supplemented by up to two canonical T gates. Compared with the counterpart based on the empirical mean, the MSE is larger by about 30%, but the overall behavior is almost the same. Similar results apply to other numerical simulations. So our main conclusions do not change if the empirical mean is replaced by the median of means.

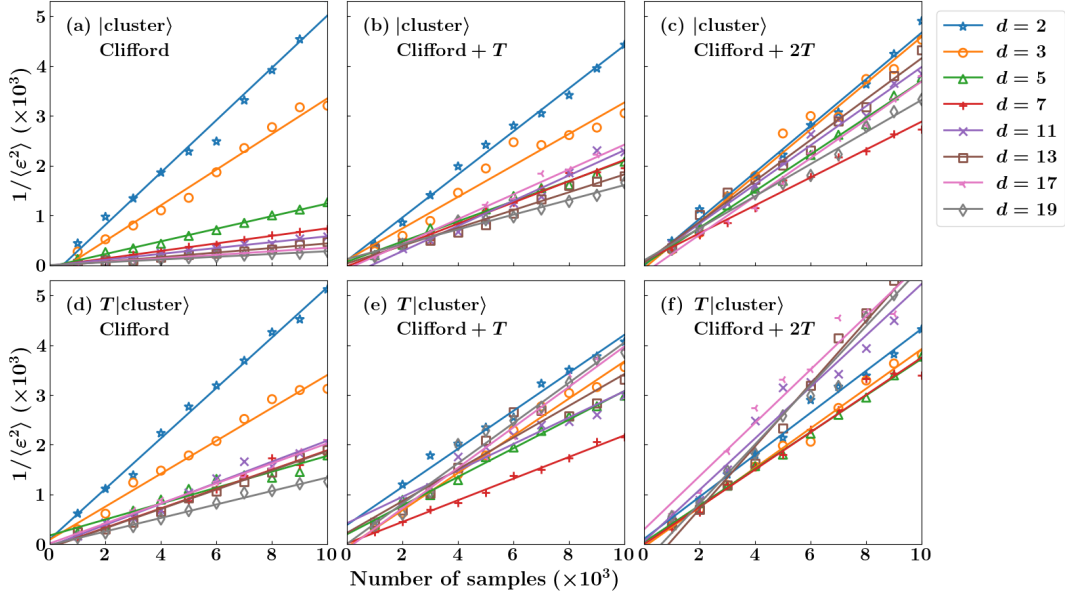


FIG. 9. Simulation results on the inverse MSE in estimating the fidelity of the 100-qudit cluster state $|\text{cluster}\rangle$ defined on a 10×10 square lattice with periodic boundary condition. The estimation protocols are based on the Clifford circuit supplemented by up to two canonical T gates. The MSE $\langle \varepsilon^2 \rangle$ for each data point is the average over 100 runs. The solid lines are determined by interpolation. Results on the state $T|\text{cluster}\rangle$ are also shown for comparison.

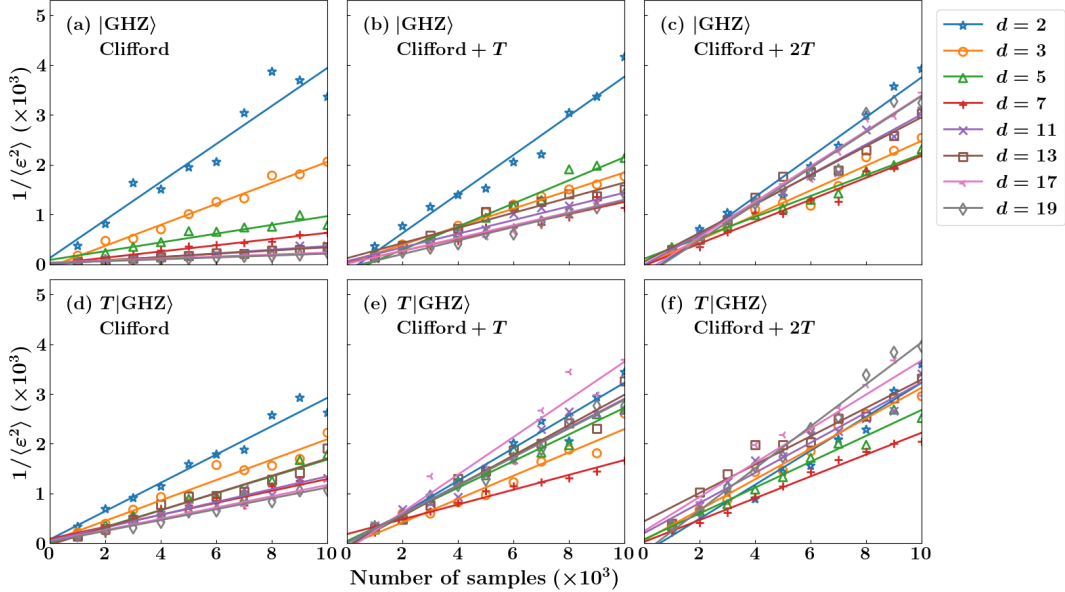


FIG. 10. Simulation results on the inverse MSE in estimating the fidelity of the 100-qudit GHZ state $|\text{GHZ}\rangle$ using the median of means estimation with $L = 10$. Here the raw data are the same as that employed in Fig. 4. The MSE $\langle \varepsilon^2 \rangle$ for each data point is the average over 100 runs, and the solid lines are determined by interpolation as before. Results on the state $T|\text{GHZ}\rangle$ are also shown for comparison.

Appendix G: Details of numerical simulation

Classical simulation of a quantum circuit has long been an important task for verification and validation of quantum devices. Notably, the Gottesman-Knill theorem states that a stabilizer circuit can be efficiently simulated on a classical computer. Later on, Aaronson and Gottesman proposed a practical simulation

algorithm [51]. Using the tableau representation, their algorithm runs in time $\mathcal{O}(n^2)$ for both deterministic and random measurements, and in time $\mathcal{O}(n^3)$ for computing the inner product between two stabilizer states, where n is the qubit number [51]. In the past two decades, several alternative approaches have been introduced, including simulation methods based on the graph state representation [59] and canonical forms of Clifford unitaries [60]. In addition, a number of sampling algorithms for the Clifford group have been proposed [54, 61, 62]. The subgroup algorithm in Ref. [54] was later generalized to the qudit setting [55]. However, as far as we know, no explicit algorithm for simulating qudit stabilizer circuits has been implemented so far.

Towards the simulation of universal quantum circuits, a number of works have studied the simulation of (qubit) stabilizer circuits interleaved by magic gates. Currently, there are two main approaches for dealing with magic gates: the first one is based on gadgetization [52, 53], and the second one is based on low-rank stabilizer decomposition [63]. For both approaches, the computational cost is polynomial in the qubit number and exponential in the number of magic gates.

Here we develop a complete simulation algorithm for qudit shadow estimation based on the Clifford group supplemented by T gates. When no T gates are involved, the data acquisition phase is essentially a random Clifford circuit. To simulate such a circuit, we generalize the tableau method proposed in Ref. [51] to the qudit setting and combine it with the Clifford sampling algorithm proposed in Ref. [55]. To deal with the addition of T gates, we then generalize the gadgetization method in Refs. [52, 53] to the qudit setting. The simulation algorithm we develop here may be useful to studying various other problems in quantum information processing and is thus of interest beyond the focus of this work.

1. Generating matrices of qudit stabilizer states

Before formulating the simulation algorithm, we need a convenient representation of qudit stabilizer states and stabilizer projectors, assuming that the local dimension d is an odd prime. Here we first introduce a representation based on generating matrices, which is the basis for more sophisticated representation methods.

Suppose $|\Psi\rangle \in \text{Stab}(n, d)$ is an n -qudit stabilizer state, and S_1, S_2, \dots, S_n form a minimal generating set of its stabilizer group. The i th stabilizer generator can be expressed as follows,

$$S_i = \chi(r_i^u) W_{\mathbf{u}_i} = \chi(r_i^u) \bigotimes_{k=1}^n W(u_{i,k}^z, u_{i,k}^x), \quad (\text{G1})$$

where the (column) vector $\mathbf{u}_i := (u_{i,1}^z, \dots, u_{i,n}^z, u_{i,1}^x, \dots, u_{i,n}^x)^\top$ is the *stabilizer vector* of $|\Psi\rangle$ associated with S_i and r_i^u is the corresponding *phase exponent*. The *generating matrix* \mathcal{G} of $|\Psi\rangle$ (with respect to the given generating set) is composed of such stabilizer vectors and phase exponents as follows,

$$\mathcal{G} = [\mathcal{G}^z | \mathcal{G}^x | r] = \left[\begin{array}{ccc|ccc|c} u_{1,1}^z & \cdots & u_{1,n}^z & u_{1,1}^x & \cdots & u_{1,n}^x & r_1^u \\ \vdots & \ddots & \vdots & \vdots & \ddots & \vdots & \vdots \\ u_{n,1}^z & \cdots & u_{n,n}^z & u_{n,1}^x & \cdots & u_{n,n}^x & r_n^u \end{array} \right], \quad (\text{G2})$$

where \mathcal{G}^z and \mathcal{G}^x encode the exponents of Z and X , respectively, while $r = r(\mathcal{G})$ encodes the phase exponents. The submatrix of \mathcal{G} excluding the last column is called the *reduced generating matrix* and denoted by $\tilde{\mathcal{G}}$ henceforth.

For the convenience of the following discussion, we use $\text{len}(\mathcal{G})$ to denote the number of rows in \mathcal{G} and use $\langle \mathcal{G} \rangle$ as a shorthand for the stabilizer group $\langle S_1, S_2, \dots, S_n \rangle$. Note that $|\Psi\rangle$ and its stabilizer group are uniquely determined by the generating matrix \mathcal{G} . According to the properties of stabilizer generators, if we swap two rows of \mathcal{G} , add one row to another, or multiply one row by any number in $\mathbb{F}_d^\times := \mathbb{F}_d \setminus \{0\}$, we get another generating matrix (with respect to a different generating set) of the same stabilizer state $|\Psi\rangle$. We shall call these ‘row operations’.

Recall that any Clifford unitary $C \in \text{Cl}(n, d)$ has the form $C = W_{\mathbf{a}\mu}(M)$ with $\mathbf{a} \in \mathbb{F}_d^{2n}$ and $M \in \text{Sp}(2n, d)$ up to an overall phase factor [see Eq. (B12)]. According to Eq. (B13), applying the Clifford unitary C on $|\Psi\rangle$ is equivalent to updating the generating matrix \mathcal{G} via the mapping

$$\mathbf{u}_i \mapsto M\mathbf{u}_i, \quad r_i^u \mapsto r_i^u + [\mathbf{a}, M\mathbf{u}_i], \quad i = 1, 2, \dots, n. \quad (\text{G3})$$

In numerical simulation of shadow estimation based on the Clifford group, we need to sample a random Clifford unitary. In the generating-matrix representation, this task amounts to sampling a random symplectic matrix $M \in \text{Sp}(2n, d)$ and a random symplectic vector $\mathbf{a} \in \mathbb{F}_d^{2n}$. Here we use the algorithm proposed in Ref. [55] for

sampling a symplectic matrix, which is a generalization of the subgroup algorithm for $\text{Sp}(2n, 2)$ proposed in Ref. [54]. The sampling of a symplectic vector is straightforward.

The above results can be generalized to stabilizer projectors in a straightforward way. Notably, a stabilizer projector of rank 2^j can be represented by a generating matrix with $n - j$ rows. By convention all rows of the generating matrix are linearly independent, and similarly for the reduced generating matrix.

2. Tableau representation of qudit stabilizer states

The generating matrix offers a very simple representation of stabilizer states, but it is not so convenient for computing the inner product and for simulating a quantum measurement. To circumvent this problem, here we turn to a more sophisticated representation, which contains valuable additional information and is very convenient in numerical simulation. The *tableau* \mathcal{J} of a stabilizer state $|\Psi\rangle \in \text{Stab}(n, d)$ is a $2n \times (2n + 1)$ matrix over \mathbb{F}_d . The upper half of \mathcal{J} is exactly the generating matrix \mathcal{G} . The lower half of \mathcal{J} is composed of n row vectors of the form $[\mathbf{v}_j^\top | r_j^y]$, where the vectors $\mathbf{v}_j \in \mathbb{F}_d^{2n}$ satisfy the following relations on symplectic inner products [51],

$$[\mathbf{u}_i, \mathbf{u}_j] = 0, \quad [\mathbf{v}_i, \mathbf{v}_j] = 0, \quad [\mathbf{u}_i, \mathbf{v}_j] = \delta_{ij}, \quad i, j = 1, 2, \dots, n; \quad (\text{G4})$$

they are called *destabilizer vectors* henceforth. The destabilizer vectors \mathbf{v}_j and corresponding phase exponents r_j^y satisfy the same update rule as \mathbf{u}_i and r_i^u as presented in Eq. (G3). In addition, they determine n Weyl operators as follows,

$$D_j := \chi(r_j^v) W_{\mathbf{v}_j} = \chi(r_j^v) \bigotimes_{k=1}^n W(v_{j,k}^z, v_{j,k}^x), \quad j = 1, 2, \dots, n, \quad (\text{G5})$$

which are called *destabilizer generators*, in contrast with the n stabilizer generators S_j for $j = 1, 2, \dots, n$. Apparently, row operations on the upper (or lower) half of the tableau \mathcal{J} do not change the underlying stabilizer state $|\Psi\rangle$.

For the convenience of the following discussion, the submatrix of \mathcal{J} composed of the first $2n$ columns is called the *reduced tableau* of $|\Psi\rangle$ and is denoted by $\tilde{\mathcal{J}}$.

3. Representation of qudit stabilizer states using Lagrangian subspaces and characteristic vectors

Stabilizer states can also be represented using Lagrangian subspaces [55, 56], which are very useful for computing the inner products between stabilizer states. Recall that a subspace \mathcal{V} of \mathbb{F}_d^{2n} is a *Lagrangian subspace* if \mathcal{V} has dimension n and the symplectic product vanishes in this subspace. Let \mathcal{V} be a subspace of \mathbb{F}_d^{2n} , the symplectic complement of \mathcal{V} is defined as

$$\mathcal{V}^\perp := \{\mathbf{v} \in \mathbb{F}_d^{2n} \mid [\mathbf{u}, \mathbf{v}] = 0 \ \forall \mathbf{u} \in \mathcal{V}\}. \quad (\text{G6})$$

Note that $\mathcal{V}^\perp = \mathcal{V}$ iff \mathcal{V} is a Lagrangian subspace.

Now, suppose $\mathbf{u}_1, \mathbf{u}_2, \dots, \mathbf{u}_n$ are n linearly independent stabilizer vectors of a stabilizer state $|\Psi\rangle \in \text{Stab}(n, d)$; then $\mathcal{L} = \text{span}(\mathbf{u}_1, \mathbf{u}_2, \dots, \mathbf{u}_n)$ is a Lagrangian subspace. In addition, there exists a vector $\mathbf{m} \in \mathbb{F}_d^{2n}$, called a *characteristic vector*, such that $|\Psi\rangle$ can be expressed as follows [56],

$$|\Psi\rangle = |\mathcal{L}, \mathbf{m}\rangle := |\mathcal{L}|^{-1} \sum_{\mathbf{u} \in \mathcal{L}} \chi([\mathbf{m}, \mathbf{u}]) W_{\mathbf{u}}. \quad (\text{G7})$$

Note that the choice of \mathbf{m} is not unique: given another vector \mathbf{m}' in \mathbb{F}_d^{2n} , then $|\mathcal{L}, \mathbf{m}'\rangle$ and $|\mathcal{L}, \mathbf{m}\rangle$ represent the same stabilizer state iff $\mathbf{m}' - \mathbf{m} \in \mathcal{L}$. Therefore, the characteristic vector \mathbf{m} has a d^n -fold degeneracy. Based on the above representation, we can simulate the Clifford transformation $C = W_{\mathbf{a}\mu}(M)$ by the following map

$$\mathbf{u}_i \mapsto M\mathbf{u}_i, \quad \mathbf{m} \mapsto M\mathbf{m} + \mathbf{a}. \quad (\text{G8})$$

In addition, the overlap between two stabilizer states $|\mathcal{L}_1, \mathbf{m}_1\rangle$ and $|\mathcal{L}_2, \mathbf{m}_2\rangle$ reads [55]

$$|\langle \mathcal{L}_1, \mathbf{m}_1 | \mathcal{L}_2, \mathbf{m}_2 \rangle|^2 = \begin{cases} d^{\dim|\mathcal{L}_1 \cap \mathcal{L}_2| - n} & \text{if } \mathbf{m}_1 - \mathbf{m}_2 \in (\mathcal{L}_1 \cap \mathcal{L}_2)^\perp \\ 0 & \text{otherwise.} \end{cases} \quad (\text{G9})$$

Based on this result, we can also simulate the measurement process.

To apply the above representation in numerical simulation, we need to determine a characteristic vector \mathbf{m} of the stabilizer state $|\Psi\rangle$ given the generating matrix in Eq. (G2). Observe that \mathbf{m} should satisfy the underdetermined system of linear equations

$$[\mathbf{m}, \mathbf{u}_i] = r_i^u \quad \forall i = 1, 2, \dots, n, \quad (\text{G10})$$

which can be solved by Gaussian elimination. This task can be greatly simplified if the destabilizer vectors \mathbf{v}_i of $|\Psi\rangle$ associated with the stabilizer vectors \mathbf{u}_i are available, in which case $\mathbf{m} = -\sum_i r_i^u \cdot \mathbf{v}_i$ is an ideal choice for the characteristic vector.

4. Simulation of stabilizer circuits

Here we introduce a simple algorithm for simulating random qudit stabilizer circuits based on the tableau representation, which generalizes the original simulation algorithm tailored to qubits [51]. To this end, first we develop an algorithm for constructing the tableau representation for an arbitrary qudit stabilizer state. Inspired by the representation of stabilizer states based on Lagrangian subspaces [55, 56], then we develop a method based on Gaussian elimination for computing the inner product and simulating the computational basis measurement, which runs in time $\mathcal{O}(n^3)$. The overall simulation algorithm in data acquisition phase is presented in Algorithm 1 below. The sampling of a random symplectic matrix in $\text{Sp}(2n, d)$ is described in detail in Section 5.3.1 of Ref. [55], which we shall not repeat here. Other relevant notations and subroutines are introduced in the following subsections.

Algorithm 1: Data acquisition for stabilizer circuit

Input : Stabilizer vectors $\mathbf{s}_1, \mathbf{s}_2, \dots, \mathbf{s}_n$ and phase exponents p_1, p_2, \dots, p_n of the input state $|\Psi\rangle$
Output: n -dit measurement outcome \mathbf{x}

- 1 Construct a tableau \mathcal{J} ; // See Appendix G4 a
- 2 Sample a random $M \in \text{Sp}(2n, d)$ and $\mathbf{a} \in \mathbb{F}_d^n$;
- 3 Update \mathcal{J} with M and \mathbf{a} ; // See Appendix G2
- 4 Sample an outcome \mathbf{x} in the computational basis measurement // See Appendix G4 b

a. Tableau construction

Suppose $|\Psi\rangle \in \text{Stab}(n, d)$ is a stabilizer state whose stabilizer group is generated by the n stabilizer operators $\chi(p_1)W_{\mathbf{s}_1}, \chi(p_2)W_{\mathbf{s}_2}, \dots, \chi(p_n)W_{\mathbf{s}_n}$, where $\mathbf{s}_1, \mathbf{s}_2, \dots, \mathbf{s}_n \in \mathbb{F}_d^{2n}$ and $p_1, p_2, \dots, p_n \in \mathbb{F}_d$ are the corresponding stabilizer vectors and phase exponents. Let $\mathcal{L} = \text{span}(\mathbf{s}_1, \mathbf{s}_2, \dots, \mathbf{s}_n)$ be the Lagrangian subspace associated with $|\Psi\rangle$. Based on this information we can construct a tableau representation \mathcal{J} of $|\Psi\rangle$ in two steps: (1) constructing stabilizer and destabilizer vectors; (2) tracking the phase exponents.

(1) Constructing stabilizer and destabilizer vectors: In this step, we want to find n stabilizer vectors $\mathbf{u}_1, \mathbf{u}_2, \dots, \mathbf{u}_n$ and n destabilizer vectors $\mathbf{v}_1, \mathbf{v}_2, \dots, \mathbf{v}_n$ that satisfy Eq. (G4) and such that $\{\mathbf{u}_i\}_{i=1}^n$ spans the same Lagrangian subspace as $\{\mathbf{s}_i\}_{i=1}^n$. This is achieved by Algorithm 2 introduced below. Let \mathcal{L}_0 be the Lagrangian subspace associated with the basis state $|0\rangle^{\otimes n}$. The basic idea of Algorithm 2 can be summarized as follows: find a symplectic transformation that maps \mathcal{L}_0 to \mathcal{L} , then the desired stabilizer vectors $\mathbf{u}_1, \mathbf{u}_2, \dots, \mathbf{u}_n$ and destabilizer vectors $\mathbf{v}_1, \mathbf{v}_2, \dots, \mathbf{v}_n$ of $|\Psi\rangle$ can be constructed by applying the same symplectic transformation to the standard stabilizer vectors and destabilizer vectors of $|0\rangle^{\otimes n}$. The overall computational complexity of Algorithm 2 is $\mathcal{O}(n^3)$.

The desired symplectic transformation can be expressed as a product of some elementary symplectic transformations known as symplectic transvections [55]. Given a vector $\mathbf{h} \in \mathbb{F}_d^{2m}$ (in our case $m = 1, 2, \dots, n$) and a scalar $\lambda \in \mathbb{F}_d^\times$, a symplectic transvection $T_{\lambda, \mathbf{h}}$ on \mathbb{F}_d^{2m} can be defined via the map

$$T_{\lambda, \mathbf{h}}(\mathbf{x}) = \mathbf{x} + \lambda[\mathbf{x}, \mathbf{h}]\mathbf{h}. \quad (\text{G11})$$

The inverse transvection reads $T_{\lambda, \mathbf{h}}^{-1} = T_{-\lambda, \mathbf{h}}$. It is well known that symplectic transvections can generate the whole symplectic group. More concretely, given any two nonzero vectors \mathbf{x}, \mathbf{y} in \mathbb{F}_d^{2m} , there exist two vectors $\mathbf{h}_1, \mathbf{h}_2 \in \mathbb{F}_d^{2m}$ and scalars $\lambda_1, \lambda_2 \in \mathbb{F}_d$ such that

$$\mathbf{y} = T_{\lambda_1, \mathbf{h}_1} T_{\lambda_2, \mathbf{h}_2}(\mathbf{x}). \quad (\text{G12})$$

This is Lemma 5.1 in Ref. [55], which also offers a constructive proof. So it should be clear how the subroutine ‘find transvections’ in Algorithm 2 works. To simplify the description, the product $T_{\lambda_1, \mathbf{h}_1} T_{\lambda_2, \mathbf{h}_2}$ is abbreviated as T in the pseudocode. Here we take the ‘local’ convention, which means the $(2j-1)$ th and $2j$ th entries of \mathbf{u} denote the powers of Z_j and X_j respectively. Let $\mathbf{e}_{2m}(i) \in \mathbb{F}_d^{2m}$ be the column vector with the i th entry equal to 1 and all other entries equal to 0. Note that the symplectic products in Eq. (G4) are preserved under symplectic transformations. In each iteration in Algorithm 2, we have $[\mathbf{u}_j^{(i+1)}, \mathbf{e}_{2(n+1-i)}(1)] = 0$ for $j = i+1, i+2, \dots, n$, which means the second entry of $\mathbf{u}_j^{(i+1)}$ must be zero. In addition, we can set the first entry to zero without changing the Lagrangian subspace of interest. Furthermore, we can discard the first two entries and continue to look for transvections that correspond to symplectic transformations in $\text{Sp}(2(n-i), d)$ in the next iteration.

Algorithm 2: Constructing the reduced tableau

Input : Stabilizer vectors $\mathbf{s}_1, \mathbf{s}_2, \dots, \mathbf{s}_n$
Output: Stabilizer vectors $\mathbf{u}_1, \mathbf{u}_2, \dots, \mathbf{u}_n$ and destabilizer vectors $\mathbf{v}_1, \mathbf{v}_2, \dots, \mathbf{v}_n$

- 1 Set $\{\mathbf{u}_1^{(1)}, \dots, \mathbf{u}_n^{(1)}\} = \{\mathbf{s}_1, \mathbf{s}_2, \dots, \mathbf{s}_n\}$;
- 2 **for** $i = 1 : n$ **do**
- 3 Find transvections and construct T_i such that $T_i \mathbf{e}_{2(n+1-i)}(1) = \mathbf{u}_i^{(i)}$;
- 4 **for** $j = i+1 : n$ **do**
- 5 $\mathbf{u}_j^{(i+1)} = T_i^{-1} \mathbf{u}_j^{(i)}$ and discard the first two entries of $\mathbf{u}_j^{(i+1)}$;
- 6 **end**
- 7 **end**
- 8 $M = T_n$ **for** $i = (n-1) : 1$ **do**
- 9 $M = T_i(\mathbb{1}_2 \oplus M)$ ($M = \mathbb{1}_2$ for $i = n$);
- 10 **end**
- 11 $\mathbf{u}_1, \mathbf{u}_2, \dots, \mathbf{u}_n$ and $\mathbf{v}_1, \mathbf{v}_2, \dots, \mathbf{v}_n$ correspond to the first n columns and last n columns of M , respectively.

(2) Tracking phase exponents: Now we determine the phase exponents in the last column of the tableau \mathcal{J} . Note that $\mathcal{L} = \text{span}(\mathbf{s}_1, \mathbf{s}_2, \dots, \mathbf{s}_n) = \text{span}(\mathbf{u}_1, \mathbf{u}_2, \dots, \mathbf{u}_n)$, and every \mathbf{s}_i can be expressed as a linear combination of $\mathbf{u}_1, \mathbf{u}_2, \dots, \mathbf{u}_n$ as follows, $\mathbf{s}_i = \sum_{j=1}^n c_i^j \mathbf{u}_j$, where

$$c_i^j = [\mathbf{s}_i, \mathbf{v}_j]. \quad (\text{G13})$$

Therefore, the phase exponents $r_1^u, r_2^u, \dots, r_n^u$ in the last column of \mathcal{J} should satisfy the following system of linear equations,

$$\sum_{j=1}^n c_i^j r_j^u = p_i, \quad (i = 1, 2, \dots, n), \quad (\text{G14})$$

which can be solved in time $\mathcal{O}(n^3)$ by Gaussian elimination. The phase exponents $\{r_i^v\}_{i=1}^n$ associated with destabilizer vectors are actually redundant. For simplicity, we set as convention $r_i^v = 0$ for $i = 1, 2, \dots, n$.

b. Computational basis measurement

The simulation of a computational basis measurement can be seen as a variant of computing the inner product of two stabilizer states. For this task it is more convenient to use the representation based on Lagrangian subspaces and characteristic vectors. For the convenience of the following discussion, here we come back to the ‘global’ convention.

Algorithm 3: Simulation of the computational basis measurement

Input : The Lagrangian subspace \mathcal{L} and characteristic vector \mathbf{m} of pre-measurement state
Output: Measurement outcome \mathbf{x}

- 1 Find a basis $\{\mathbf{w}_k\}_{k=1}^{\zeta}$ of $\mathcal{L}_0 \cap \mathcal{L}$ with the Zassenhaus algorithm;
- 2 Construct the equations according to Eq. (G16), and solve for $\tilde{\mathbf{x}}$;
- 3 Return the latter half of $\tilde{\mathbf{x}}$ as \mathbf{x} .

Suppose the stabilizer state before the measurement is $|\Psi_f\rangle = |\mathcal{L}, \mathbf{m}\rangle$, where \mathcal{L} and \mathbf{m} are the corresponding Lagrangian subspace and characteristic vector. The outcome of the computational basis measurement can be labeled by a vector \mathbf{x} in \mathbb{F}_d^n , which corresponds to the basis state $|\mathbf{x}\rangle$. This basis state can also be expressed as $|\mathbf{x}\rangle = |\mathcal{L}_0, \tilde{\mathbf{x}}\rangle$, where \mathcal{L}_0 is the Lagrangian subspace associated with the computational basis and is spanned by the n vectors $\mathbf{e}_{2n}(1), \mathbf{e}_{2n}(2), \dots, \mathbf{e}_{2n}(n)$, and the characteristic vector $\tilde{\mathbf{x}}$ can be chosen to be $\tilde{\mathbf{x}} = (\mathbf{0}; \mathbf{x})$. If we perform the computational basis measurement on the stabilizer state $|\mathcal{L}, \mathbf{m}\rangle$, then the probability of obtaining outcome \mathbf{x} reads

$$p(\mathbf{x}) = |\langle \mathcal{L}, \mathbf{m} | \mathcal{L}_0, \tilde{\mathbf{x}} \rangle|^2. \quad (\text{G15})$$

Next, we introduce a scheme for sampling the n -dit measurement outcome \mathbf{x} . First, construct a basis $\{\mathbf{w}_k\}_{k=1}^{\zeta}$ for $\mathcal{L}_0 \cap \mathcal{L}$ using the Zassenhaus algorithm [64] for example, where $\zeta = \dim|\mathcal{L}_0 \cap \mathcal{L}|$ and $0 \leq \zeta \leq n$. Choose $n - \zeta$ vectors $\mathbf{y}_1, \mathbf{y}_2, \dots, \mathbf{y}_{n-\zeta}$ in \mathbb{F}_d^{2n} such that $\{\mathbf{w}_k\}_{k=1}^{\zeta} \cup \{\mathbf{y}_k\}_{k=1}^{n-\zeta}$ forms a basis for \mathcal{L}_0 . Then we can sample the measurement outcome \mathbf{x} by solving the system of linear equations

$$\begin{aligned} [\tilde{\mathbf{x}}, \mathbf{w}_i] &= [\mathbf{m}, \mathbf{w}_i] \quad \text{for } i = 1, 2, \dots, \zeta, \\ [\tilde{\mathbf{x}}, \mathbf{y}_j] &= c_j \quad \text{for } j = \zeta + 1, \zeta + 2, \dots, n, \end{aligned} \quad (\text{G16})$$

where each c_j is a random number in \mathbb{F}_d . Finally, we take the latter half of $\tilde{\mathbf{x}}$, which is exactly \mathbf{x} . The overall procedure is summarized in Algorithm 3.

5. Simulation of Clifford circuits supplemented by T gates

In the main text, we focus on fidelity estimation using shadow estimation as a prototypical task. In this section, we shall describe how to classically simulate the procedure when the unitary ensemble corresponds to a random Clifford circuit supplemented by T gates.

In the data acquisition stage, an input state goes through a layer of random Clifford gate $C_0 \in \text{Cl}(n, d)$, a layer of T gates, and a layer of Fourier gates, followed by the computational basis measurement. If the input state can be prepared from $|0\rangle^{\otimes n}$ with a few layers of Clifford and T gates, then this procedure can be efficiently simulated. That is to say, we can sample the measurement outcome $\mathbf{x} := (x_1, x_2, \dots, x_n)^\top \in \mathbb{F}_d^n$ of this quantum circuit according to the probability distribution $\{p(\mathbf{x})\}_{\mathbf{x}}$ on a classical computer, with computational cost polynomial in n and exponential in $t = t_1 + t_2$, where t_1 is the number of T gates used in state preparation, and t_2 is the number of T gates in the unitary ensemble.

a. Reverse gadgetization

To simulate the circuit mentioned above, we generalize the gadgetization method in Ref. [53] to the qudit setting. For simplicity, we denote each diagonal magic gate liberally as T , regardless of its specific type. For each T gate we can define a single-qudit magic state $|T^\dagger\rangle$ according to Eq. (D2). Then the T gate can be replaced equivalently by a ‘reversed’ gadget, which can be expressed diagrammatically as follows,

$$\begin{array}{c} \text{---} \bullet \text{---} \\ | \\ \oplus \\ \text{---} |0\rangle \end{array} = \boxed{\frac{1}{\sqrt{d}} T}. \quad (\text{G17})$$

Circuits in this section are read from right to left, so that we can derive the expressions of intermediate quantum states directly from the circuit diagram.

Suppose the input state is $C_1 T^{\otimes s_1} \otimes C_2 T^{\otimes s_2} \dots C_{l-1} T^{\otimes s_{l-1}} C_l |0\rangle^{\otimes n}$, where $\sum_{i=1}^{l-1} s_i = t_1$ and $C_1, C_2, \dots, C_l \in \text{Cl}(n, d)$, then the circuit U we are to simulate can be expressed diagrammatically as in the upper plot in Fig. 11. We assume that the t_2 T gates in the measurement primitive are applied to the first t_2 qudits without loss of generality. Since C_0 is selected randomly from $\text{Cl}(n, d)$, C_1 can be absorbed into C_0 . The equivalent circuit based on reverse gadgetization is shown in the lower plot in Fig. 11.

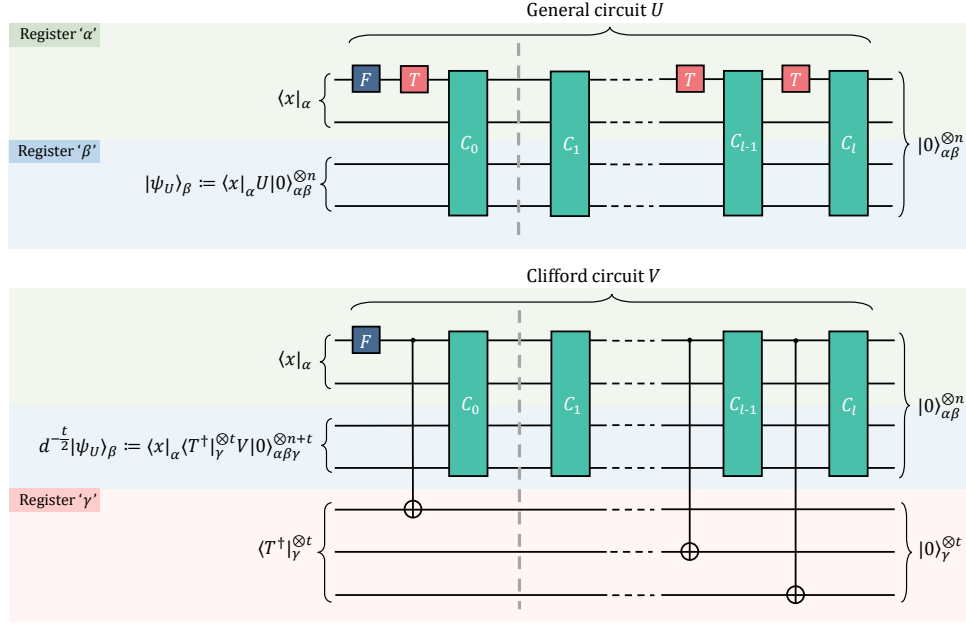


FIG. 11. (upper) A Clifford circuit interleaved by T gates. The gates on the right of the vertical dashed line are used to prepare the input state, while the gates on the left are used to realize a random quantum measurement employed in shadow estimation. (lower) The post-selected circuit obtained after reverse gadgetization of all T gates.

b. Main simulation algorithm

To sample the outcome \mathbf{x} , we sample the outcome on each qudit sequentially [52], in which the sampling on the j th qudit with $j = 2, 3, \dots, n$ is determined by the conditional probabilities

$$p(y | x_1, \dots, x_{j-1}) := \frac{p(x_1, \dots, x_{j-1}, y)}{p(x_1, \dots, x_{j-1})}, \quad y \in \mathbb{F}_d. \quad (\text{G18})$$

In this way, to simulate each experimental shot, we need to calculate the outcome probabilities $p(\mathbf{x})$ for only nd sequences \mathbf{x} of length varying from 1 to n , instead of all d^n probabilities $p(\mathbf{x})$ for $\mathbf{x} \in \mathbb{F}_d^n$.

Next, we illustrate how to evaluate the outcome probability $p(\mathbf{x})$ for the outcome $\mathbf{x} = (x_1, \dots, x_m)^\top$ of a measurement on the first m qudits with $1 \leq m \leq n$. For the convenience of the following discussion, the first m qudits are referred to as the measured register ‘ α ’, and the remaining $(n - m)$ qudits are referred to as the marginalized register ‘ β ’; the identity operators on registers α and β are denoted by \mathbb{I}_α and \mathbb{I}_β , respectively. Then the probability $p(\mathbf{x})$ can be expressed as follows,

$$p(\mathbf{x}) = \|\langle \mathbf{x} |_\alpha U |0\rangle_{\alpha\beta}^{\otimes n}\|_2^2. \quad (\text{G19})$$

After gadgetization, the circuit U acting on $|0\rangle_{\alpha\beta}^{\otimes n}$ is re-expressed as a Clifford circuit V acting on $|0\rangle_{\alpha\beta\gamma}^{\otimes n+t}$, with t ancillary qudits in register ‘ γ ’ post-selected on the state $|T^\dagger\rangle$. Thus the above probability can be expressed as

$$p(\mathbf{x}) = d^t \|\langle \mathbf{x} |_\alpha \langle T^\dagger |_\gamma^{\otimes t} V |0\rangle_{\alpha\beta\gamma}^{\otimes n+t}\|_2^2 = d^t \text{tr}(\Pi_{\mathcal{G}_0} \Pi_{\mathbf{x}, T}), \quad (\text{G20})$$

where \mathcal{G}_0 is the generating matrix of the stabilizer state $V |0\rangle_{\alpha\beta\gamma}^{\otimes n+t}$ and

$$\Pi_{\mathcal{G}_0} = V |0\rangle_{\alpha\beta\gamma}^{\otimes n+t} V^\dagger, \quad \Pi_{\mathbf{x}, T} = |\mathbf{x}\rangle \langle \mathbf{x}|_\alpha \otimes \mathbb{I}_\beta \otimes (|T^\dagger\rangle \langle T^\dagger|)_\gamma^{\otimes t}. \quad (\text{G21})$$

Let

$$\Lambda_{\mathbf{x}, \gamma} = \text{tr}_{\alpha\beta} [\Pi_{\mathcal{G}_0} (|\mathbf{x}\rangle \langle \mathbf{x}|_\alpha \otimes \mathbb{I}_{\beta\gamma})], \quad (\text{G22})$$

where $\mathbb{I}_{\beta\gamma}$ is the identity operator on registers β and γ together. Then the probability $p(\mathbf{x})$ can be expressed as $p(\mathbf{x}) = \text{tr}[\Lambda_{\mathbf{x},\gamma}(|T^\dagger\rangle\langle T^\dagger|_\gamma^{\otimes t})]$. If the partial trace in Eq. (G22) does not vanish, then $\Lambda_{\mathbf{x},\gamma}$ is proportional to a stabilizer projector $\Pi_{\mathcal{G}_{\mathbf{x},\gamma}}$ acting on register γ , where $\mathcal{G}_{\mathbf{x},\gamma}$ is a generating matrix. Eventually, $p(\mathbf{x})$ can be expressed as follows,

$$p(\mathbf{x}) = \begin{cases} d^{\xi-m} \text{tr} [\Pi_{\mathcal{G}_{\mathbf{x},\gamma}(|T^\dagger\rangle\langle T^\dagger|_\gamma^{\otimes t})}], & \text{if } flag = \text{True}, \\ 0, & \text{if } flag = \text{False}. \end{cases} \quad (\text{G23})$$

The generating matrix $\mathcal{G}_{\mathbf{x},\gamma}$ and relevant parameters can be determined by virtue of Algorithm 5 in Appendix G 5 c. After obtaining $\mathcal{G}_{\mathbf{x},\gamma}$, the probability $p(\mathbf{x})$ can be computed directly in time $\mathcal{O}(td^{k_\gamma+1})$ with $k_\gamma = \text{len}(\mathcal{G}_{\mathbf{x},\gamma}) \leq t$, where t is the total number of single-qudit magic states employed in the simulation; the computational cost usually increases exponentially with t .

The procedure for simulating a Clifford circuit supplemented by T gates is summarized in Algorithm 4. Naive implementation of Algorithm 4 results in a time complexity of $\mathcal{O}(nd(n+t)^3 + ntd^{t+2})$. However, we can make some optimization by reusing some intermediate results, which can reduce the complexity to $\mathcal{O}((n+t)^3 + (nd+t)d^{t+1})$.

Algorithm 4: Data acquisition for Clifford circuits supplemented by T gates

Input : Circuit representation of U
Output: n -dit measurement outcome \mathbf{x}

- 1 Construct the generating matrix \mathcal{G}_0 for $|0\rangle^{\otimes n}$, apply $C_l, \text{CNOT}, C_{l-1}, \dots$ sequentially;
- 2 Sample a random $M \in \text{Sp}(2n, d)$ and $\mathbf{a} \in \mathbb{F}_d^{2n}$;
- 3 Update \mathcal{G}_0 with M and \mathbf{a} ;
- 4 Update \mathcal{G}_0 according to the actions of CNOT and F gates on the relevant qudits;
- 5 **for** $m = 1 : n$ **do**
- 6 **for** $y = 0 : d - 1$ **do**
- 7 $\mathbf{y} = \text{concatenate}(\mathbf{x}, y)$;
- 8 $flag, \xi, \mathcal{G}_{\mathbf{x},\gamma} = \text{Constrain stabilizers}(\mathcal{G}_0, \mathbf{y})$;
- 9 **if** $flag = \text{True}$ **then**
- 10 $p(\mathbf{y}) = d^{\xi-m} \text{tr} [\Pi_{\mathcal{G}_{\mathbf{x},\gamma}(|T^\dagger\rangle\langle T^\dagger|_\gamma^{\otimes t})}]$;
- 11 **else**
- 12 $p(\mathbf{y}) = 0$;
- 13 **end**
- 14 **end**
- 15 Sample \mathbf{y} according to $\{p(\mathbf{y})/p(\mathbf{x})\}_{y=0}^{d-1}$, $\mathbf{x} \leftarrow \mathbf{y}$;
- 16 **end**
- 17 **return** \mathbf{x}

In principle, the stabilizer circuits discussed in the previous section can also be simulated using Algorithm 4 with some minor modification. When the number of T gates to be gadgetized is $t = 0$, the outcome probability $p(\mathbf{x})$ is given directly by Algorithm 5 as

$$p(\mathbf{x}) = \begin{cases} d^{\xi-m}, & \text{if } flag = \text{True}, \\ 0, & \text{if } flag = \text{False}. \end{cases} \quad (\text{G24})$$

The corresponding time complexity for sampling one-dit outcome is $\mathcal{O}(n^3)$, and the overall complexity for sampling an n -dit outcome \mathbf{x} is approximately $\mathcal{O}(n^4d)$ by naive implementation. By reusing some intermediate results, we can reduce the overall complexity to $\mathcal{O}(n^3)$, but it is still not as efficient as the tableau method in Appendix G 4. In addition, when no T gates are involved, it is much more efficient to calculate the inner product between two stabilizer states using Lagrangian subspaces and characteristic vectors.

c. Partial trace of stabilizer projectors

In this subsection we describe how to compute the partial trace in Eq. (G22), which corresponds to the step ‘Constrain stabilizers’ in Algorithm 4. To this end, we need to introduce some additional notations. For any Weyl operator $W = \omega_d^j W_{u_1} \otimes \dots \otimes W_{u_n} \in \mathcal{W}(n, d)$ with $j \in \mathbb{F}_d$ and $u_1, \dots, u_n \in \mathbb{F}_d^2$, we use $|W\rangle_i$ to denote

the i th tensor factor W_{u_i} and $\omega(W)$ to denote the phase factor ω_d^j . In addition, we use $|W|_\alpha$ to denote the sub-string of tensor factors associated with register ' α ', that is, $|W|_\alpha := \bigotimes_{i=1}^m W_{u_i}$, and similarly for $|W|_\beta$ and $|W|_\gamma$.

In order to contribute non-trivially to the partial trace in Eq. (G22), a stabilizer operator $W \in \langle \mathcal{G}_0 \rangle$ must satisfy the following constraints:

1. $|W|_i = I$ for each qudit in register ' β ', that is, $m+1 \leq i \leq n$.
2. $|W|_i \in \{I, Z, \dots, Z^{d-1}\}$ for each qudit in register ' α ', that is, $1 \leq i \leq m$.

Note that the subset of stabilizer operators in $\langle \mathcal{G}_0 \rangle$ that satisfy the above two constraints also forms a stabilizer group. Let \mathcal{G}_2 be a generating matrix associated with the resulting stabilizer group and $\Pi_{\mathcal{G}_2}$ the corresponding stabilizer projector. Let $\xi = \text{len}(\mathcal{G}_2)$ be the number of rows of \mathcal{G}_2 and let S_j be the stabilizer operator associated with the j th row of \mathcal{G}_2 . Then $\Lambda_{\mathbf{x}, \gamma}$ in Eq. (G22) can be expressed as follows,

$$\begin{aligned} \Lambda_{\mathbf{x}, \gamma} &= \text{tr}_{\alpha\beta} [\Pi_{\mathcal{G}_0}(|\mathbf{x}\rangle\langle \mathbf{x}|_\alpha \otimes \mathbb{I}_{\beta\gamma})] = d^{\xi-n-t} \text{tr}_{\alpha\beta} [\Pi_{\mathcal{G}_2}(|\mathbf{x}\rangle\langle \mathbf{x}|_\alpha \otimes \mathbb{I}_{\beta\gamma})] \\ &= d^{-m-t} \sum_{W \in \langle \mathcal{G}_2 \rangle} h_{\mathbf{x}}(W) = d^{-m-t} \prod_{j=1}^{\xi} \sum_{k_j \in \mathbb{F}_d} h_{\mathbf{x}}(S_j^{k_j}), \end{aligned} \quad (\text{G25})$$

where $h_{\mathbf{x}}$ is a function from the stabilizer group $\langle \mathcal{G}_2 \rangle$ to the Pauli group on register γ ,

$$h_{\mathbf{x}}(W) := d^{m-n} \text{tr}_{\alpha\beta} [W(|\mathbf{x}\rangle\langle \mathbf{x}|_\alpha \otimes \mathbb{I}_{\beta\gamma})] = \omega(W) \langle \mathbf{x} | |W|_\alpha | \mathbf{x} \rangle |W|_\gamma. \quad (\text{G26})$$

Note that $\Lambda_{\mathbf{x}, \gamma} = 0$ whenever there exists a stabilizer operator $W \in \langle \mathcal{G}_2 \rangle$ such that $h_{\mathbf{x}}(W) = \omega^k \mathbb{I}_\gamma$ for some $k \in \mathbb{F}_d^\times$, where \mathbb{I}_γ is the identity operator on register γ .

Now, suppose the first $2(n+t)$ columns of \mathcal{G}_2 have been turned into an inverse echelon form. Then $\Lambda_{\mathbf{x}, \gamma} = 0$ iff $h_{\mathbf{x}}(S_j) = \omega^k \mathbb{I}_\gamma$ for some stabilizer generator S_j and $k \in \mathbb{F}_d^\times$. If such a stabilizer generator does not exist, then $\Lambda_{\mathbf{x}, \gamma}$ is proportional to the stabilizer projector associated with the following set of stabilizer generators acting on register γ ,

$$\{h_{\mathbf{x}}(S_j) : h_{\mathbf{x}}(S_j) \neq \mathbb{I}_\gamma\}, \quad (\text{G27})$$

which can be encoded by a generating matrix $\mathcal{G}_{\mathbf{x}, \gamma}$. Based on this observation we can devise an efficient algorithm for computing the partial trace in Eq. (G25) and for determining the generating matrix $\mathcal{G}_{\mathbf{x}, \gamma}$. Before presenting the algorithm, it is convenient to introduce three useful functions.

(1) Slicing of \mathcal{G} : We denote by $\mathcal{G}^z[i:j, k:l]$ the sub-matrix of \mathcal{G}^z that contains rows from i to j and columns from k to l , and similarly for $\mathcal{G}^x[i:j, k:l]$. For \mathcal{G} we define

$$\mathcal{G}[i:j, k:l] := \left[\begin{array}{ccc|ccc|c} u_{i,k}^z & \cdots & u_{i,l}^z & u_{i,k}^x & \cdots & u_{i,l}^x & r_i^u \\ \vdots & \ddots & \vdots & \vdots & \ddots & \vdots & \vdots \\ u_{j,k}^z & \cdots & u_{j,l}^z & u_{j,k}^x & \cdots & u_{j,l}^x & r_j^u \end{array} \right]. \quad (\text{G28})$$

When the argument in position i (k) is omitted, we mean starting from the first row (column). When the argument in position j (l) is omitted, we mean stopping on the last row (column). Suppose $i < j$, $k < l$, $\mathcal{G}[j:i, k:l]$ means rearranging the rows of $\mathcal{G}[i:j, k:l]$ in inverse order, and $\mathcal{G}[i:j, l:k]$ means rearranging the columns of $\mathcal{G}[i:j, k:l]$, except for the last column, in inverse order. In any case, $\tilde{\mathcal{G}}[i:j, k:l]$ denotes the submatrix of $\mathcal{G}[i:j, k:l]$ without the last column, while $r(\mathcal{G})[i:j]$ denotes the last column of $\mathcal{G}[i:j, k:l]$, that is,

$$\tilde{\mathcal{G}}[i:j, k:l] := \left[\begin{array}{ccc|ccc} u_{i,k}^z & \cdots & u_{i,l}^z & u_{i,k}^x & \cdots & u_{i,l}^x \\ \vdots & \ddots & \vdots & \vdots & \ddots & \vdots \\ u_{j,k}^z & \cdots & u_{j,l}^z & u_{j,k}^x & \cdots & u_{j,l}^x \end{array} \right], \quad r(\mathcal{G})[i:j] := \begin{bmatrix} r_i^u \\ \vdots \\ r_j^u \end{bmatrix}. \quad (\text{G29})$$

(2) Echelon forms of \mathcal{G} : We denote by *Echelon*(\mathcal{G}, k) (*Echelon-z*(\mathcal{G}, k), *Echelon-x*(\mathcal{G}, k)) the generating matrix \mathcal{G}' obtained by row operations (swap, addition, and multiplication by integers in \mathbb{F}_d^\times) on the generating matrix \mathcal{G} such that $\tilde{\mathcal{G}}'[:, 1:k]$ ($\mathcal{G}'^z[:, 1:k]$, $\mathcal{G}'^x[:, 1:k]$) is in echelon form. In addition, we denote by *inv-Echelon*(\mathcal{G}, k) (*inv-Echelon-z*(\mathcal{G}, k), *inv-Echelon-x*(\mathcal{G}, k)) the generating matrix \mathcal{G}' obtained by row operations on \mathcal{G} such that $\tilde{\mathcal{G}}'[:, k:1]$ ($\mathcal{G}'^z[:, k:1]$, $\mathcal{G}'^x[:, k:1]$) is in echelon form.

(3) The cut function for (inverse) echelon form: When \mathcal{G}^z is in echelon form (or inverse echelon form), $cut\text{-}z(\mathcal{G}; k, l)$ is defined as the smallest row index j of \mathcal{G} such that $\mathcal{G}^z[j, k:l]$ has all entries equal to zero. In a similar way, we can define $cut\text{-}x(\mathcal{G}; k, l)$ and $cut(\tilde{\mathcal{G}}; k, l)$ by replacing \mathcal{G}^z with \mathcal{G}^x and $\tilde{\mathcal{G}}$, respectively; in addition, we set $cut(\mathcal{G}; k, l) = cut(\tilde{\mathcal{G}}; k, l)$.

As an illustration of the above functions, we can transform \mathcal{G} into *Echelon-x* form and then take the rows of \mathcal{G} with index $j \geq cut\text{-}x(\mathcal{G}; k, l)$ to form a new generating matrix \mathcal{G}' . In this way we can make sure that $|W|_i \in \{I, Z, \dots, Z^{d-1}\}$ for $W \in \langle \mathcal{G}' \rangle$ and $k \leq i \leq l$. By applying similar procedures twice, we can construct the aforementioned generating matrix \mathcal{G}_2 .

The procedure for computing the partial trace in Eq. (G25) and for determining the generating matrix $\mathcal{G}_{\mathbf{x}, \gamma}$ is summarized in Algorithm 5. Since the most time-consuming part is the construction of echelon forms of generating matrices, which is based on Gaussian elimination, the time complexity of Algorithm 5 is approximately $\mathcal{O}((n+t)^3)$. Note that some intermediate results featuring in Algorithm 5, including the generating matrices \mathcal{G}_1 and \mathcal{G}_2 , can be used repeatedly in the sampling algorithm, namely, Algorithm 4. Based on this observation we can optimize our sampling algorithm, so as to reduce the time complexity.

Algorithm 5: Constrain stabilizers

Input : Generating matrix \mathcal{G}_0 , m -dit outcome \mathbf{x}
Output: Boolean *flag*, integer ξ , constrained stabilizers $\mathcal{G}_{\mathbf{x}, \gamma}$

- 1 $\mathcal{G}_0 \leftarrow \text{Echelon-x}(\mathcal{G}_0, n+t)$;
- 2 $c_1 = cut\text{-}x(\mathcal{G}_0; 1, n)$, $\mathcal{G}_1 = \mathcal{G}_0[c_1 :, :]$;
- 3 $\mathcal{G}_1 \leftarrow \text{inv-Echelon-z}(\mathcal{G}_1, n)$;
- 4 $c_2 = cut\text{-}z(\mathcal{G}_1; m+1, n)$, $\mathcal{G}_2 = \mathcal{G}_1[c_2 :, :]$;
- 5 $\mathcal{G}_2 \leftarrow \text{inv-Echelon}(\mathcal{G}_2, n+t)$;
- 6 $c_3 = cut(\mathcal{G}_2; n+1, n+t)$;
- 7 $r(\mathcal{G}_2) \leftarrow r(\mathcal{G}_2) + \mathcal{G}_2^z[:, :m] \cdot \mathbf{x}$;
- 8 **if** $r(\mathcal{G}_2)[c_3 :]$ *contains non-zero entries* **then**
- 9 | *flag* = False
- 10 **else**
- 11 | *flag* = True
- 12 **end**
- 13 $\mathcal{G}_{\mathbf{x}, \gamma} = \mathcal{G}_2[c_3 - 1, n+1 : n+t]$;
- 14 **return** *flag*, $\xi = \text{len}(\mathcal{G}_2)$, $\mathcal{G}_{\mathbf{x}, \gamma}$
